RADIATION FROM TENSILE FRACTURES

by

LALATENDU MANSINHA
B.Sc., Indian Institute of Technology, 1957
M.Tech., Indian Institute of Technology, 1959

A THESIS SUBMITTED IN PARTIAL FULFILMENT OF
THE REQUIREMENTS FOR THE DEGREE OF

DOCTOR OF PHILOSOPHY

in the Department

of

PHYSICS

We accept this thesis as conforming to the
required standard

THE UNIVERSITY OF BRITISH COLUMBIA

October, 1962

In presenting this thesis in partial fulfilment of the requirements for an advanced degree at the University of British Columbia, I agree that the Library shall make it freely available for reference and study. I further agree that permission for extensive copying of this thesis for scholarly purposes may be granted by the Head of my Department or by his representatives. It is understood that copying or publication of this thesis for financial gain shall not be allowed without my written permission.

Department of PHYSICS

The University of British Columbia,
Vancouver 8, Canada.

Date 29th October 1962

The University of British Columbia

FACULTY OF GRADUATE STUDIES

PROGRAMME OF THE

FINAL ORAL EXAMINATION

FOR THE DEGREE OF

DOCTOR OF PHILOSOPHY

of

LALATENDU MANSINHA

B.Sc., Indian Institute of Technology, 1957
M.Tech., Indian Institute of Technology, 1959

MONDAY, OCTOBER 29, 1962, at 3:30 P.M.
IN ROOM 303, PHYSICS BUILDING

COMMITTEE IN CHARGE

Chairman: F.H. Soward

M.A. Chinnery	W.F. Slawson
J.A. Jacobs	R.W. Stewart
D.L. Livesey	E. Teghtsoonian
J.C. Savage	W.H. White

External Examiner: Jean-Claude De Bremaecker
Rice University

RADIATION FROM TENSILE FRACTURES

ABSTRACT

The geographical distribution of the sense of the first motion of P waves (and to a very limited extent, S waves) has been studied by seismologists to provide information on the focal mechanism of earthquakes. In this thesis we investigate the inverse problem: knowing the type and form of displacement at the focus at the focal instant, we study the azimuthal distribution of the sense of first P and S motion, using model seismic technique. The source of elastic energy is a thermally induced tensile fracture in a glass plate. Two types of fractures have been studied: Initial (bilaterally propagating) Fractures and Extended (unilaterally propagating) Fractures. The azimuthal distribution of P and S wave amplitudes is indicated. The experiments reported in this thesis constitute a partial test of a recent theory by Knopoff and Gilbert (1960) on first motions from seismic sources. The type of fracture studied corresponds to Case 3 of Knopoff and Gilbert. Our results show significant discrepancies with the theory. The sense of the measured first S motion is opposite to that predicted by the theory, for both Initial and Extended Fractures. The ratios P_θ/P_{90} and S_θ/P_θ differ significantly in magnitude from the theory in many azimuths. It is suggested that the discrepancies are possibly due to the neglect in the theory of non-linear elastic effects near the tip of the fracture.

GRADUATE STUDIES

Field of Study: Seismology

Introduction to Quantum Mechanics	J. Grindlay
Theory of Measurements	J.R. Prescott
Nuclear Physics	J.B. Warren
Advanced Geophysics	J.A. Jacobs
Radioactive and Isotopic Processes in Geophysics	R.D. Russell
Modern Aspects of Geophysics	J.A. Jacobs

Related Studies:

Applied Electromagnetic Theory	G.B. Walker
Mineral Deposits	W.H. White

ABSTRACT

The geographical distribution of the sense of the first motion of P waves (and to a very limited extent, S waves) has been studied by seismologists to provide information on the focal mechanism of earthquakes. In this thesis we investigate the inverse problem; knowing the type and form of displacement at the focus at the focal instant, we study the azimuthal distribution of the sense of first P and S motion, using model seismic technique. The source of elastic energy is a thermally induced tensile fracture in a glass plate. Two types of fractures have been studied: Initial (Bilaterally propagating) Fractures and Extended (Unilaterally propagating) Fractures. The azimuthal distribution of the P and S wave amplitudes is indicated. The experiments reported in this thesis constitute a partial test of a recent theory by Knopoff and Gilbert (1960) on first motions from seismic sources. The type of fracture studied corresponds to Case 3 of Knopoff and Gilbert. Our results show significant discrepancies with the theory. The sense of the measured first S motion is opposite to that predicted by the theory, for both Initial and Extended Fractures. The ratios P_θ / P_{90} and S_θ / P_θ differ in magnitude from the theory in many azimuths. It is suggested that the discrepancies are possibly due to the neglect in the theory of non-linear elastic effects near the tip of the fracture.

TABLE OF CONTENTS

Page

ACKNOWLEDGEMENT

It is a pleasure to acknowledge the help I have received from Dr. James C. Savage. Dr. Savage suggested that I investigate problems of elasticity and seismology with model seismic technique, and after that devoted a considerable amount of his own time in discussing ideas and performing experiments. I have learned a lot from working with him, and I take this opportunity to express my indebtedness to him. I also thank Dr. R. D. Russell, who acted as my supervisor during Dr. Savage's absence, and Dr. J. A. Jacobs for his constant interest and encouragement during the experimental work.

This work was financially supported by grants from the American Petroleum Institute.

LIST OF FIGURES

Page

LIST OF SYMBOLS

For convenience a partial list of symbols frequently used in the text is given here. Other symbols are defined wherever they are introduced.

α	Longitudinal wave velocity.
β	Transverse wave velocity.
γ_x	Direction cosine.
ψ	Velocity of Propagation of fracture.
(r, θ)	Plane polar coordinates.
P_θ (A)	P wave recorded at (r, θ) with transducer A.
P_θ (r)	P wave amplitudes at angle θ, for different r.
E P_θ	P (R, θ) from Extended Fractures.
I P_θ	P (R, θ) from Initial Fractures.
P_θ / P_{90}	Ratio of P amplitude at (R, θ) to P amplitude at $(R, 90^\circ)$.
S_θ / P_θ	Ratio of S amplitude at (R, θ) to P amplitude at (R, θ).
S_θ (B)	S wave recorded at (r, θ) with transducer B.

LIST OF TABLES

CHAPTER I

INTRODUCTION

1.1 General.

A recent paper by Knopoff and Gilbert (1960) has predicted the radiation pattern of elastic waves associated with fractures of various types. This theory takes as a model of a fracture a dislocation in a certain component of displacement or strain; linear elasticity theory is then used to predict the earliest longitudinal and transverse motions associated with the dislocation. The work reported here consists of an experimental test of this theory, as well as a general experimental study of elastic waves from fractures of certain types.

The principal interest in the study of the radiation of elastic waves from a fracture is to apply the results to the inverse problem of inferring the properties of the fracture from the radiation pattern. This problem is of particular importance in geophysics where the direction and nature of fracture in earthquakes is not adequately known; indeed, it is possible that fracture does not play a role in some earthquakes (e.g., are deep focus earthquakes the result of a dislocation in strain rather than in displacement?). Other questions of interest concern the partitioning of energy between longitudinal

and transverse waves and the question of whether fracture tends to propagate in a single direction (unilateral fracture) or simultaneously in two opposite directions (bilateral fracture). The experiments reported here have a bearing on all of these questions.

1.2 Previous Works.

The literature on seismic sources is not extensive. Kasahara (1952 to 1955) published a series of papers on his experimental studies on the generation of elastic waves, using widely different experimental techniques. In the first paper, he used the transducing parts of a loudspeaker as a source on a block of agar-agar (72 x 33 x 13 cms). Surface motions at various distances from the source were studied with a variable capacitor type of detector. Longitudinal, transverse and surface waves were identified. He also verified a result of Lapwood, that a purely downward motion at a point on the surface is accompanied by upward motion in the immediate area surrounding the point.

In the fifth paper of this series, Kasahara simulates an explosive source. A cylindrical cavity lined with thin rubber film was embedded in a block of agar-agar 90 x 30 x 30 cms in dimensions. The dimensions of the cavity were 0.6 cms in radius and 20 cms in length. Elastic

waves were excited by an impulsive increase of pressure in the cavity with an air pump. Motion at the epicenter, and at various points away from it, were studied. Only longitudinal and surface waves were identified. The form, as well as the amplitude, of the displacement changed as one moved away from the epicenter.

Kasahara and a number of other investigators (Howes et al (1953), Tatel (1954), Evans et al (1954), Oliver et al (1954), Press et al (1954), Knopoff (1955), Levin et al (1955), O'Brien (1955), Knopoff (1956), Kato et al (1956)), have perfected the theory and technique of seismic modelling. Most of the early works were on three dimensional models, which are cumbersome and expensive to use. Oliver, Press and Ewing (1954) were the first to propose and use two dimensional models to study seismic phenomena. They established the correspondence between certain plate vibration modes and body waves.

The group velocities of symmetric and anti-symmetric plate waves have a pronounced dependance on kh, where k is the wave number and h the thickness of the plate (see appendix II). For wavelengths long in comparison with the plate thickness, kh is small and the dispersion of the first symmetric mode is small. It has been established (appendix II) that the first symmetric mode in the two dimensional model corresponds to longitudinal

body waves in three dimensions. For small kh the velocity of the asymmetrical (flexural) mode is much less than symmetric or shear modes and thus does not interfere with these modes in seismic modelling. Shear waves with displacement in the plane of the two dimensional model show no dispersion and have velocity independent of plate thickness. Oliver, Press and Ewing used a plate thickness of 1/16 inch and a frequency of the order of 10^2 kc/s.

The first attempt to study the elastic wave radiation from non-propagating faults in two-dimensional models was by Press (1956, 1957) and independently by Kato and Takagi (1957). A high voltage, short duration pulse applied to a piezo-electric bimorph transducer produces a short duration mechanical displacement. This simulates a singlet source. A properly oriented combination of such bimorph transducers can simulate any force or displacement systems acting at the focus at the focal instant. At the center of a thin circular sheet combinations of benders served to simulate singlet, doublet and quadruplet sources. Two oppositely phased benders, separated by a short distance, form a doublet source; four form a quadruplet source. By interposing a slit between the doublet benders, Press was able to simulate a fault. With silicone as a lubricant he was able to study a lubricated fault. The arms of the doublet

pointed in the 0° and 180° directions, representing a fault oriented in the same direction. The P wave distribution pattern had vanishing amplitudes at 0° and 90°, both with and without slits. But the S wave pattern changed significantly in the presence of a slit. With no slit, S amplitude is at a minimum at 0°, increasing to a maximum at 90°. In the presence of a slit, the S wave null is shifted 25° to 30° to the side from that of a simple dipole. The sense of shear motion is clockwise, in contrast to the counterclockwise motion in the 30° to 90° zone.

Later work by Healy and Press (1959) suggests that the anomalous shear distribution is due to Rayleigh waves travelling along the slit face and being converted at the termination into shear waves. This is supported by the work of Joffe (1951), who shows that a system of surface waves (not necessarily Rayleigh waves) can be found which satisfy the boundary conditions of a moving Griffith crack.

Press, Ben-Menahem and Toksoz (1961) reported a method to recover two parameters of the earthquake focus from the fault plane solution. The methods are based on the analysis of free oscillation of the earth and of long period mantle Rayleigh waves and G waves. The theoretical basis for the method has been described by Benioff, Press and Smith (1961), and Ben-Menahem (1961). Free spheroidal oscillations of the earth for high mode numbers are

equivalent to standing wave interference patterns of Rayleigh waves propagating in opposite directions. The phase shift between vertical and horizontal displacement for propagating waves is 90°, and for standing waves 180°. For a point source excitation, Rayleigh waves are excited equally in all directions, and phase shifts of 0° or 180° are produced. If the energy is radiated in only one direction, the phase shift will be 90°. For cases where radiation in opposite direction is unequal, the phase shift will assume some intermediate value. This is the case for faulting with a finite rupture velocity.

To test this theory, Press, Ben-Menahem and Toksoz used a circular aluminum plate 12" in radius and 1/16" in thickness. A sinusoidal function was used to excite the ceramic source transducer. The frequency was varied until resonance occurred. Nodes were counted by receiver at the rim of the plate. The reciprocity theorem permits the use of a moving receiver instead of a moving source. The source was kept fixed while the receiver was moved in discrete intervals of 2°. The solutions were superimposed after time shifting by an amount equal to the translation time of the source for a 2° interval. Such a composite record is approximately equivalent to a finite moving source.

A more precise method is mentioned by Press, Ben-

Menahem and Toksoz, but to date no results have been published. A moving source is simulated by a series of static ceramic source transducers pulsed in sequence, with suitable time delays between pulsing of adjacent transducers. The net impression is a source moving in discrete steps with an equivalent velocity to a continuously moving source.

1.3 Method of Investigation.

Thermal stresses are set up in a glass plate by applying an open flame to the side of the plate at a point about 1½ cm from, and along the extension of, a 1/2 cm linear scratch previously inscribed on the plate (see fig.1). When sufficient tensile stress builds up across the scratch, a fracture initiates at the scratch and propagates along its prolongation. The sudden displacement associated with the fracture gives rise to symmetric plate waves (hereafter termed 'P', to distinguish from P waves in three dimensions) and transverse S waves.

It should be emphasized here that the experiment is by no means a direct analogue of the problem of an initiated fracture propagating in a three dimensional body. To establish the connection between the two we will have to consider the following analogies. First, we note that the waves in the thin plate are related to waves in a three dimensional body subject to the constraint of

plane strain (i.e., vanishing components of strain across the sides of the plate). We note that in either case the significant motions are in the plane of the plate. In the unconstrained plate, however, small motions perpendicular to the plate do occur in the symmetric plate wave. These motions permit a variation of volume per unit area of the plate, whereas all variations of volume per unit area of the constrained plate come about through compression of matter. Thus the unconstrained plate may be thought of as a constrained plate having an unusually high compressibility. This analogy has been formally established by Oliver, Press and Ewing (1954). The second stage of the argument involves the juxtaposition of a very large number of the constrained plates to form a solid three dimensional body in plane strain. In order to be definite let us choose a set of cartesian axes oriented so that all motion is parallel to the X-Z plane. We imagine that the fracture propagates in the X direction. The three dimensional analogue of a fracture in a plate is then a fracture which initiates simultaneously at every point on the Y axis and propagates in the X direction so that every section parallel to the X-Z plane is at all times identical (see fig. 2). On the other hand the theory of Knopoff and Gilbert (1960) considers a fracture which has only an infinitesimal length along the Y axis and propagates along

the X axis (fig. 3). It is the latter problem which we wish to model. This leads us to the third and final step in our argument. We will restrict ourselves to observations in the X-Z plane (see fig. 3) and consider only the first motions of the longitudinal and transverse waves. We see from figure 2 that only an infinitesimal length of the fracture centered upon the origin may contribute to the first motions observed on the X-Z plane, the disturbance from the remainder of the points on the infinite fracture not having had time to reach the point of observation. (There will be, to be sure, a difference in the geometric attenuation of the wave in the two cases, the amplitude being proportional to $r^{-\frac{1}{2}}$ in our experiments and proportional to r^{-1} in the theory. This difference need not concern us here.) On the basis of these arguments we may conclude that the experiments described in this thesis should give the correct radiation pattern in the X-Z plane for the fracture depicted in figure 2. It is therefore an experimental test of the theory of Knopoff and Gilbert.

CHAPTER II

FRACTURE PHENOMENON

2.1 Definition.

We define fracture as a process by which a free surface is created in the interior of an elastic medium under the action of an internal or external stress distribution. The free surface may expand at a finite velocity; this velocity is presumably less than the longitudinal or transverse wave velocities in the medium. In general the free surface will enclose a penny shaped volume. As the two plane bounding surfaces of the penny shaped volume approach each other, the volume tends to zero, and it is possible to speak of a fracture plane. We assume that there is no relative motion of particles immediately adjacent to, and on both sides of the fracture plane before the passage of the fracture front. The passage of the fracture front then corresponds to a suddenly applied difference in displacement or strain across the fracture plane. If we assume a step function time dependence, a fracture would correspond to a propagating step function in the difference of displacement and/or strain across the fracture plane. It follows that in an ideal fracture of the type described above, all elastic wave radiation is due to action at the fracture front.

In literature the terms crack and fracture have been used as interchangeable terms to describe the existence of free surface in the medium. In this thesis we use the term 'fracture' and 'crack' for static case and 'propagating fracture' for the dynamic case. When referring to works of other authors in the field their original terminology has been maintained.

2.2 Velocity Considerations.

Joffe (1951) has shown that the stress distribution around the head of a propagating fracture can be determined by considering the fracture as a system of moving surface disturbances. The stress distribution varies with velocity. For a stationary fracture $\sigma_\theta(r,\theta)\big|_{r=R}$ (see fig. 4 for coordinate system) is a maximum some distance ahead of the crack in the direction of propagation ($\theta = 0^\circ$). It is due to this maxima of tensile stress that the fracture propagates ahead in a straight line. With increasing velocity the variation of $\sigma_\theta(r,\theta)\big|_{r=R}$ with θ decreases until at about 0.6 of the transverse wave velocity $\sigma_\theta(r,\theta)\big|_{r=R}$ is independent of θ . It is expected that at this velocity the fracture will have no preferred direction of propagation and will form branches, leading to a division of available energy of fracture formation. With formation of branches the velocity should continue to be

maintained at less than 0.6 β . Therefore we can consider 0.6 β as the limiting or maximum velocity of propagation of a tensile fracture.

There has been no other theoretical work on other types of propagating discontinuities. However, from intuitive reasoning one cannot see a method by which a fracture can propagate at velocities higher than the longitudinal wave velocity. Points away from the fracture cannot know of the existence of the fracture before a time equal to the travel time of the longitudinal wave elapses. Cases have been observed in which fractures have travelled at apparent velocities in excess of the longitudinal wave velocity. Presumably the explanation in such cases is that the high tensile stress has caused the fracture to originate at more than one nucleus, resulting in a high apparent velocity.

Schardin and Struth (1937) have experimentally verified that the maximum tensile fracture velocity in glass is 1500 m/sec, about 0.5 of the transverse wave velocity. This maximum velocity is practically independent of temperature and of the overall stress at the moment of fracture (Schardin, 1959). Glass plates with high internal stresses gave identical maximum velocity as those from which stresses have been removed. Measurement of fracture velocity in plates under high compressive loads also gave

no velocity variation with load.

We can thus establish an empirical relation between $\mathcal{S}_m$, the maximum fracture velocity and the shear wave velocity. This is

$$\mathcal{S}_m = 0.6\beta = 0.6\sqrt{\frac{\mu}{\rho}}$$

From the foregoing it would appear that a fracture may propagate at any velocity between 0 and 0.6β . During the experiments described in this thesis it was not uncommon to see fracture creep forward at velocities less than 1 mm/sec. However, there is evidence that this may only be an apparent velocity, being made up of intermittent fractures each of which advanced only a short distance but at the full velocity of 0.6β . The major evidence supporting this view is the observation of Schardin (1959) that no fracture has been observed to move at a lower velocity once it attains the maximum value. A fracture may stop suddenly after moving at a velocity of 0.6β , but within the limits of resolution of measuring instruments (1 mm, 1 μ sec) a transition to a lower velocity could not be observed.

It is of some importance to note that the fracture velocity does not depend on the thickness of the plate being used. This is also seen from the empirical relation between $\mathcal{S}_m$ and β . The transverse wave velocity β is

independent of plate thickness.

2.3 Criterion for Crack Instability.

To explain the discrepancy between the theoretical estimate of strength of solids and actual measurements Griffith (1920, 1922) suggested that the difference might be due to the presence of large number of small cracks in solids. The cracks could concentrate the stress locally such that the theoretical strength might be locally exceeded at a comparatively low mean stress. It is possible to calculate the strain energy due to the presence of a crack in a plate. The relief of strain is opposed by the energy required to create two new surfaces. It was proposed by Griffith that the crack would spread only if the decrease in strain is greater than the increase in surface energy.

Inglis (1913) calculated the stress distribution about an elliptical hole in a stressed plate. He suggested that the case in which the eccentricity approaches unity (very flat ellipse) the elliptical hole should be a good model for a crack. The change in strain energy in a large thin plate due to the presence of an elliptical crack is given by

$$W = \frac{(3-P)\,\pi c^2 T^2}{8\mu} \qquad (2\text{-}1)$$

where T = tension

$P = \frac{3-\nu}{1-\nu}$

2c = length of crack

ν = Poisson's ratio.

λ, μ = Lame's constants

In the above expression it is assumed that the crack is very narrow; i.e. the angle between the two sides of the crack is 0^{o}. As the crack propagates surface energy is created. Potential energy of the surface of the crack, per unit thickness of the plate is

$$R = 4cS \qquad \text{where } S = \text{surface tension.}$$

The total decrease of the potential energy of the system due to the presence of the crack is given by

$$- \quad W - R = \frac{(3-P)\pi c^2 T^2}{8\mu} - 4cS \qquad (2\text{-}2)$$

Griffith's condition that the crack may extend is given by

$$- \quad \frac{\partial}{\partial c}(W - R) = 0$$

or $$(3-P)\pi c T^2 = 16\mu S$$

or $$T = \sqrt{\frac{2ES}{\pi(1-\nu^2)c}} \qquad (2\text{-}3)$$

2.4 Stress Distribution Around a Static Crack.

A treatment of the static stress distribution around a stationary crack was done by Westergaard (1939) using a complex stress function. This technique was later exploited by Williams (1956) in a more complete analysis

of the problem. We give below a brief account of the method of Williams. The solution of the equations

$$\nabla^4 F(r,\psi) = 0 \qquad (2\text{-}4)$$

will give the stress function of the type

$$F(r,\psi,\lambda) = r^{\lambda+1} f(\psi,\lambda)$$

$$= r^{\lambda+1}\left[C_1 \sin(\lambda+1)\psi + C_2 \cos(\lambda+1)\psi\right.$$

$$\left. + C_3 \sin(\lambda-1)\psi + C_4 \cos(\lambda-1)\psi\right] \qquad (2\text{-}5)$$

The above stress function will satisfy conditions of stress free edges at $\psi = 0$ and $\psi = \alpha$ if the λ are chosen as the positive roots of

$$\sin(\lambda\alpha) = \pm \lambda \sin\alpha$$

For the case where $\alpha = 2\pi$, corresponding to the case of a crack with flank angle $\varphi = \alpha - 2\pi = 0$ the above equation takes the form $\sin 2\pi\lambda = 0$, thus requiring $\lambda = n/2$, where n = 1,2,3, ... and giving the stress function

$$F(r,\psi,n/2) = r^{n/2+1}\left[C_1 \sin(n/2+1)\psi + C_2 \cos(n/2+1)\psi\right.$$

$$\left. + C_3 \sin(n/2-1)\psi + C_4 \cos(n/2-1)\psi\right] \qquad (2\text{-}6)$$

Solving the equations Williams obtained the solutions for the stress as

$$\sigma_r(r,\theta) = \frac{1}{4r^{\frac{1}{2}}}\left[a_1\left\{-5\cos\frac{\theta}{2} + \cos\frac{3\theta}{2}\right\}\right. \qquad \text{where } \Theta = \psi - \pi$$

$$\left. + \; b_1\left\{-5\sin\frac{\theta}{2} + 3\sin\frac{3\theta}{2}\right\}\right]$$

$$+ \; 4a_2\sin^2\Theta \; + \; O(r^{\frac{1}{2}}) + \ldots . \qquad (2\text{-}7)$$

$$\sigma_\theta(r,\theta) = \frac{1}{4r^{\frac{1}{2}}}\left[a_1\left\{-3\cos\frac{\theta}{2} - \cos\frac{3\theta}{2}\right\}\right.$$

$$\left. + \; b_1\left\{-3\sin\frac{\theta}{2} - 3\sin\frac{3\theta}{2}\right\}\right]$$

$$+ \; 4a_2\sin^2\Theta \; + \; O(r^{\frac{1}{2}}) + \ldots . \qquad (2\text{-}8)$$

$$\tau_{r,\theta}(r,\theta) = \frac{1}{4r^{\frac{1}{2}}}\left[a_1\left\{-\sin\frac{\theta}{2} - \sin\frac{3\theta}{2}\right\}\right.$$

$$+ b_1\left\{\cos\frac{\theta}{2} + 3\cos\frac{3\theta}{2}\right\}$$

$$\left. - 2a_2 \sin 2\theta + O(r^{\frac{1}{2}}) + \cdots\right] \quad (2\text{-}9)$$

For convenience the solution can be treated in two parts, the symmetric case when $b_i = 0$ and the anti-symmetric case when $a_i = 0$. In both cases a characteristic square root singularity is obtained. The symmetric crack is more common, being observed in plates under tension. Some interesting observations can be made from the results by Williams. Firstly, at $\theta = 0$, along the axis of the crack the shear stress vanishes, making σ_r and σ_θ the principal stresses. The values of σ_r and σ_θ are given by

$$\sigma_r(0^\circ) = \sigma_\theta(0^\circ) = -a_1 r^{-\frac{1}{2}} + \cdots$$

This means that a state of two dimensional hydrostatic tension exists near the end of a crack, along its axis.

2.5 Stresses Around a Propagating Fracture.

The work of Joffe (1951) on the stress distribution around the head of a propagating fracture has been mentioned before in this chapter. We propose to give here a brief account of her method and results.

Consider a crack of length 2c in a thin infinite plate. If the plate is under a sufficiently large transverse tension T, the crack may be expected to propagate. For large 2c the stress distributions at the ends of the crack will be independent of each other. By keeping the crack of constant length the problem reduces to that of a plate under uniform tension across which a disturbance (the crack) passes at a constant speed. We define our coordinate system such that the X-Y plane is the plane of the plate, and the crack propagates in the positive X direction. The tension T acts in the Y direction. The boundary conditions are

$$\left.\begin{aligned} \sigma_x &= 0 \\ \sigma_y &= T \\ \sigma_{xy} &= 0 \end{aligned}\right\} \quad \text{at} \quad \infty$$

$$\sigma_y = \sigma_{xy} = 0 \quad \text{on } y = 0,\ -c < x < c$$

Considering separately the moving part of the system, with T removed we have

$$\sigma_y = -T \qquad \text{on } y = 0, \quad -c < x < c$$

$$\sigma_{xy} = 0$$

The symmetry permits us to consider only the upper half plane. Defining u_x and u_y as the displacements, and

$x' = x - \varsigma t$ where ς is the velocity of fracture propagation

the boundary conditions for a dynamic elastic system are

$$\sigma_y = -T \qquad \text{at } y = 0 \qquad -c < x' < c$$

$$\sigma_{xy} = 0 \qquad \text{at } y = 0 \qquad \text{all } x'$$

$$u_y = 0 \qquad \text{at } y = 0 \qquad |x'| > c$$

These boundary conditions have to be satisfied by surface disturbances propagating at a velocity ς without displacement in the Z direction. Such disturbances can be represented by

$$u_{x_1} = A_s \exp(-\tau s y) \sin sx'$$

$$u_{y_1} = A_s \tau \exp(-\tau s y) \cos sx' \qquad (2\text{-}10)$$

$$u_{x_2} = B_s \eta \exp(-\eta s y) \sin sx'$$

$$u_{y_2} = B_s \exp(-\eta s y) \cos sx' \qquad (2\text{-}10)$$

Here $$\gamma^2 = 1 - \frac{\varsigma^2}{\alpha^2}$$

$$\eta^2 = 1 - \frac{\varsigma^2}{\beta^2}$$

Displacements of the above type vanish rapidly with the increase of y, if s is positive. Using the condition

$$\sigma_{xy} = \mu \left(\frac{\partial u_x}{\partial y} + \frac{\partial u_y}{\partial x} \right) = 0 \qquad \text{on } y = o$$

we obtain the relation

$$B_s = - \frac{2\gamma}{1+\eta^2} A_s$$

The general form of the displacement is given by integrating the expressions

$$u_x = u_{x_1} + u_{x_2}$$

$$u_y = u_{y_1} + u_{y_2}$$

over all positive values of S.

Thus

$$u_x = \int_0^\infty A_s \left[\exp(-\tau s y) - \frac{2\eta\tau}{1+\eta^2} \exp(-\eta s y) \right] \sin sx' \, ds$$

and

$$u_y = \int_0^\infty \tau A_s \left[\exp(-\tau s y) - \frac{2}{1+\eta^2} \exp(-\eta s y) \right] \cos sx' \, ds$$

Substitution of the above expression into

$$\sigma_x = (\lambda + 2\mu) \frac{\partial u_x}{\partial x} + \lambda \frac{\partial u_y}{\partial y} \qquad \text{etc.}$$

will give expressions for the various stress components. The unknown A_s is determined from the boundary conditions. From the relation

$$\sigma_\theta = \sigma_x \sin^2\theta + \sigma_y \cos^2\theta - 2\sigma_{xy} \sin\theta \cos\theta$$

one can determine the hoop stress at constant r and different θ. The origins of the polar coordinate system (r, θ) are at $x = c$ and $y = 0$. In figure 5 we reproduce from Joffe (1951) the variation of σ_θ with θ for various φ. For low φ the hoop stress distribution shows a maximum in the direction of the crack at $\theta = 0^\circ$. The variation of σ_θ with θ decreases with increase of φ until at about 0.6β, σ_θ does not change with θ. For $\varphi < 0.6\beta$ therefore the fracture propagates in a

straight line. But when ς approaches 0.6β the fracture has no preferred direction of propagation as nearly equal stresses exist over a wide range of angles ahead of the fracture.

2.6 Radiation from a Propagating Fracture.

An integral of the elastic wave equation given by Knopoff (1956) and de Hoop (1958) has been used by Knopoff and Gilbert (1960) to determine the first motion radiation pattern from various types of propagating dislocations. Consider a volume V bounded by two surfaces S' as shown in figure 6. In the limiting case the outer surface is expanded until it goes to infinity and the inner surface is shrunk until it reduces to the fault plane. The inner surface, the fault plane, is oriented so that the normal coincides with the Z axis in a cartesian system. It should be noted here that for the surfaces S' the outwardly drawn normal is the positive direction. The $+$ and $-$ superscript and subscript after the stress and displacement tensors represent the differences in these terms between the positive and negative Z sides of the fault.

We assume that, 1) there are no body forces inside the volume V; 2) that the only surface pertinent to the problem is interior to the infinite elastic medium

and 3) we are interested only in the first motions (the high frequency solution) from the impulsive excitation of the surface S′ by suddenly applied discontinuities in the stress tensor τ_{ij} or the displacement tensor p_{ij}. We follow here the terminology and definitions of Knopoff and Gilbert (1960).

For clarity we define here certain quantities:

Displacement = u_i

Stress tensor τ_{ij} = $(\alpha^2 - 2\beta^2)\, u_{k,k}\delta_{ij} + \beta^2 (u_{i,j} + u_{j,i})$

Displacement tensor p_{ij} = $(\alpha^2 - 2\beta^2)\, n_k u_k \delta_{ij} + \beta^2 (n_i u_j + n_j u_i)$

Retardation with P velocity = $\left[u(t)\right] = u(t - r/\alpha)$

Retardation with S velocity = $\left\langle u(t) \right\rangle = u(t - r/\beta)$

Coordinates of the point of observation = (x, y, z) and (r, θ)

Coordinates of a point on the fault plane = (x', y', z')

Distance r = $\left\{(x'-x)^2 + (y'-y)^2 + (z'-z)^2\right\}^{1/2}$

Direction cosines γ_i = $(x_i - x_i')/r$

In the X-Z plane the direction cosines of r = $\gamma_x = (x - x')/r = \cos\theta$

$\gamma_z = (z - z')/r = \sin\theta$

The differential equation of motion of a homogeneous isotropic elastic medium is

$$\alpha \text{ grad div } U - \beta \text{ curl curl } U - \frac{\partial U}{\partial t} = f/\rho$$

where f/ρ is the body force density. The solution of this equation by Knopoff and de Hoop is

$$\ddot{u}_i(x,y,z) = \int_v G_{ij} f_j \, dv' + \int_s G_{ij} n_m \tau_{mj} \, ds' - \int_s \frac{\partial}{\partial x'_k} G_{ij} p_{jk} \, ds' \tag{2-12}$$

where the operator G_{ij} is defined by

$$4\pi G_{ij}\Phi = \left\{\frac{1}{\alpha^2}\left[K_\alpha \Phi\right] - \frac{1}{\beta^2}\left\langle K_\beta \Phi \right\rangle\right\} \gamma_i \gamma_j + \delta_{ij}\left\{-\frac{1}{\alpha^2}\left[L_\alpha \Phi\right] + \frac{1}{\beta^2}\left\langle L_\beta \Phi \right\rangle + \frac{\langle \ddot{\Phi} \rangle}{\beta^2 r}\right.$$

$$K_\alpha = \frac{1}{r}\frac{\partial^2}{\partial t^2} + \frac{3\alpha}{r^2}\frac{\partial}{\partial t} + \frac{3\alpha^2}{r^3}$$

$$L_\alpha = \frac{\alpha}{r^2}\frac{\partial}{\partial t} + \frac{\alpha^2}{r^3} \quad ; \quad \ddot{\Phi} = \frac{\partial^2 \Phi}{\partial t^2}$$

(2-13)

In the absence of body forces, and noting that the unit normal vector on S' pointing into V is negative we have

$$\ddot{u}(x,y,z) = -\int_s G_{ij} \tau_{zj}^{+} \, ds' - \int_s \frac{\partial}{\partial x'_k} G_{ij} p_{jk}^{+} \, ds' \tag{2-14}$$

The operator G_{ij} is approximated for large r by neglecting terms involving $1/r^2$ and $1/r^3$

$$4\pi G_{ij} = \frac{1}{\alpha^2 r}\left[\ddot{\Phi}\right]\gamma_i\gamma_j + \frac{1}{\beta^2 r}\langle\ddot{\Phi}\rangle(\delta_{ij} - \gamma_i\gamma_j) \qquad (2\text{-}15)$$

and P_{ij} is

$$= -(\alpha^2 - 2\beta^2)\, u_z\, \delta_{ij} + \beta^2(u_i\,\delta_{jz} + u_j\,\delta_{iz})$$

The motion at a remote point can be written as the sum of P wave motion and the S wave motion. Thus

$$4\pi\alpha^2 u_{iP}(x,y,z) = -\int_S \frac{1}{r}\left[\ddot{\tau}_{zj}\right]^+_- \gamma_i\gamma_j\, ds' - \int_S \frac{\partial}{\partial x'_k}\left[\dot{\dot{p}}_{jk}\right]^+_- \frac{\gamma_i\gamma_j}{r}\, ds' \qquad (2\text{-}16)$$

$$4\pi\beta^2 u_{iS}(x,y,z) = -\int_S \frac{1}{r}\left\langle\ddot{\tau}_{zj}\right\rangle^+_-(\delta_{ij} - \gamma_i\gamma_j)\, ds' - \int_S \frac{\partial}{\partial x'_k}\left\{\left\langle\dot{p}_{jk}\right\rangle^+_-(\delta_{ij} - \gamma_i\gamma_j)\right\} ds' \qquad (2\text{-}17)$$

For first motions at large r we may write

$$\frac{\partial}{\partial x'_k}\left\{\left[\dot{p}_{jk}\right]^+_- \frac{\gamma_i\gamma_j}{r}\right\} \approx \frac{\gamma_i\gamma_j}{r}\,\frac{\partial}{\partial x'_k}\left[\dot{p}_{jk}\right]^+_- \qquad (2\text{-}18)$$

as the second term in the differentiation falls off as r^2.

The disturbance at large r may be considered as originating from a point, even though the point propagates along the fault plane. For first motions we are interested in a very small range of time, and within this interval the discontinuities may be considered to be substantially uniform over the surface S', eliminating the need for

integration over ds'.

It must be noted here that the stress and displacement tensors used here differ from the standard definitions of these quantities by certain dimensions of velocity and density. We change the dimensions of τ_{ij} and p_{ij} to now include the elemental area ds'. Since these are constant factors they will not affect the calculated radiation pattern.

The expressions for u_{ip} and u_{is} then become

$$4\pi\alpha^2 u_{ip}(x,y,z) = \frac{\gamma_i\gamma_j}{r}\left[\ddot{\tau}_{zj}\right]^{+}_{-} - \frac{\gamma_i\gamma_j}{r}\frac{\partial}{\partial x'_k}\left[\dot{p}_{jk}\right]^{+}_{-} \qquad (2\text{-}19)$$

$$4\pi\beta^2 u_{is}(x,y,z) = \frac{\delta_{ij}-\gamma_i\gamma_j}{r}\left\langle\ddot{\tau}_{zj}\right\rangle^{+}_{-} - \frac{\delta_{ij}-\gamma_i\gamma_j}{r}\frac{\partial}{\partial x'_k}\left\langle\dot{p}_{jk}\right\rangle^{+}_{-} \qquad (2\text{-}20)$$

In polar coordinates the above equations become

$$4\pi\alpha^2\tilde{u}_p = \tilde{r}_i\frac{\gamma_j}{r}\left[w_j\right]^{+}_{-}$$

$$4\pi\beta^2\tilde{u}_s = \tilde{\theta}_j\frac{s_j}{r}\left\langle w_j\right\rangle^{+}_{-} \qquad (2\text{-}21)$$

where

$$w_j = -(\alpha^2-2\beta^2)\epsilon_{kk}\delta_{jz} - 2\beta^2\epsilon_{jz} + (\alpha^2-2\beta^2)\frac{\partial}{\partial x'_k}u_z\delta_{jk}$$

$$+\beta^2\frac{\partial}{\partial x'_k}(u_k\delta_{jz} + u_j\delta_{kz})$$

The vector $\tilde{r}_i$ is a unit vector in the radial direction and $\tilde{\theta}_j$ is a unit vector in a direction at right angles to $\tilde{r}_i$ and lies in a plane containing $\tilde{e}_j$ and $\tilde{r}_i$, and pointing in the positive direction from e_j to $\tilde{r}_i$. The unit vector in the j direction is $\tilde{e}_j$. The sine of the angle between $\tilde{e}_j$ and $\tilde{r}_i$ is given by

$$s_j = (1 - \gamma_j^2)^{\frac{1}{2}}$$

An actual fault or fracture may be a combination of all or some of the terms in the expression w_j. Knopoff and Gilbert have determined the first motion radiation pattern by considering each of the terms of w_j in turn, and assuming the other seven to be zero. For a step function time dependance we can write

$$\epsilon_{ij}^{+}_{-} = H(t - x'/\varsigma)\, H(x')$$

and

$$u_i = H(t - x'/\varsigma)\, H(x')$$

The fault propagates in the x direction with velocity ς. $H(\varphi)$ is the unit step function.

For a tensile fracture of the type considered in this thesis all terms in w_j except u_z are zero. Then w_j is equal to

$$w_j = (\alpha^2 - 2\beta^2)\frac{\partial u_z}{\partial x'}, (\alpha^2 - 2\beta^2)\frac{\partial u_z}{\partial y'}, \alpha^2 \frac{\partial u_z}{\partial z'}$$

Noting that $\frac{\partial}{\partial x'} H(t - r/\alpha) = \frac{\gamma_x}{r} \delta(t - r/\alpha)$, we obtain, on the X-Z plane

$$4\pi \tilde{u}_p = \frac{\tilde{r}_1}{r} \left\{ \frac{1}{\alpha} + \frac{(2\beta^2 - \alpha^2)}{\alpha^2 \varsigma} \cos\theta - \frac{2\beta^2}{\alpha^3} \cos^2\theta \right\} \qquad (2\text{-}22)$$

$$4\pi \tilde{u}_s = \frac{\tilde{\theta}_x}{r} \left\{ - \frac{\sin 2\theta}{\beta} - \frac{(\alpha^2 - 2\beta^2)}{\beta^2 \varsigma} \sin\theta \right\} \qquad (2\text{-}23)$$

Knopoff and Gilbert appear to have overlooked the direction of the normal to S'. This changes the sign of the first integral in their equation (2) and the sign of σ_{ij} given just below that equation. There appear to be some further errors in sign which partly, but not completely, cancel the previous error. Our equations for the displacements caused by a type 3 dislocation (in Knopoff and Gilbert's nomenclature) differ from their equation (12) in the sign of all terms containing ς and in the inclusion of s_x in the first term of the second of the two equations. This latter is clearly only a typographical error.

CHAPTER III

INSTRUMENTATION AND EXPERIMENTAL TECHNIQUE

3.1 Scaling Considerations.

Knopoff (1955) shows that in seismic models the relationship

$$g = t \quad \text{and} \quad p = v = 1$$

should hold. Here g is the geometrical scale factor, p the Poisson's ratio scale factor, t the time scale factor, and v the velocity scale factor. In this thesis our primary aim is to study the far field radiation of a moving source. Therefore we do not have to conform to the rigid scaling considerations. We must, however, satisfy the thin plate restrictions and also record sufficiently far from the fracture so that only the far field is detected. The thin plate and the far field requirements oppose each other. The far field condition means that observations be made a large number of wavelengths away from the source. For finite plate dimensions this condition can be achieved only with small wavelengths. On the other hand, thin plate theory requires that the wavelength be long compared with the plate thickness.

In the series of experiments described here we have used a plate thickness of 3 mm, with measured P' wave

velocity of 5500 m/sec and an S wave velocity of 3700 m/sec. At a frequency of 100 kc/s the wavelengths are

$$\lambda_\alpha = 5.5 \text{ cms} \quad \text{and} \quad \lambda_\beta = 3.7 \text{ cms.}$$

Thus the wavelengths are much greater than the plate thickness. Most of the observations have been made at distances greater than 25 cms from the source. In order to verify that the measurements were not influenced by the near field, an attempt was made to measure the geometric attenuation of the elastic waves from the fracture. For two dimensional waves the amplitude should vary as $r^{-\frac{1}{2}}$ in the far field, but in the near field the amplitude should fall off more rapidly. Details of the experiment are given in section 4.5. The measured exponent of r came out to be $- 0.53 \pm 0.08$ (Standard Error). It is felt that the experimental result verifies that measurements at distances greater than 20 cms do not involve near field to any appreciable extent.

3.2 Methods of Inducing Fracture.

An inhomogeneous thermal stress field is set up in the glass plate by the application of heat to a small region (see fig. 1). Because of the thermal gradient, there is differential expansion, and radial and hoop stresses are developed in the plate. As is well known,

fracture in glass is readily induced by tensile stress, and the hoop stresses are thus admirably suited to initiate fractures. If the temperature in the central heated region becomes too high, the properties of the glass will be altered, and the propagation of elastic waves in the plate may be affected. In addition, plastic yielding may take place. For the purpose of this experiment, therefore, it is important that the temperature of the heat source be sufficiently low to prevent any significant alteration of the elastic properties of glass. Temperature measurements on the glass plate after heating with a gas flame for 60 seconds gave a central heated zone of 5 mm radius at 200° C.

To determine whether this heated zone would suffice to distort the radiation pattern and arrival times of an ultrasonic wave, an experiment was devised. An ultrasonic signal was transmitted along a glass plate from a repetitive source to a pick-up transducer. The signal was filtered in exactly the same way as the signals from an actual fracture. The flame was then applied 2 cm away from the source along the line joining source and receiver. No change in the signal was observed in the two minutes that the flame was applied to the plate. There was also no detectable change in the time of arrival. It is concluded therefore that the elastic properties of the glass were

not modified by heating in a sufficient amount to distort the radiation pattern or the arrival time of the elastic waves. This is further supported by the fact that the elastic constants of the type of glass used do not change more than 3 per cent over a temperature range from 0° to 200° C.

In Appendix I calculations are shown for computing radial and hoop stresses set up by such a heated zone. The approximate temperature distribution after 45 sec of the application of the flame is shown in figure 7. The radial and hoop stress distribution set up by the temperature gradient is shown in figure 8. It is seen that the compressive radial stresses increase rapidly towards the center of the heated zone, while the tensile hoop stress reaches a maximum value at about 1.5 cm from the center of the heated zone. We have observed that the fracture does in fact originate at about 1.5 cm from the point of application of heat.

To initiate a fracture a very shallow scratch about 0.5 cm long is made on the surface of the glass sheet. Heat is applied 1.5 cm from the end of the scratch by a gas flame. After a period of build-up of stress (about 30 to 60 seconds) a fracture forms spontaneously and propagates in the direction of the scratch. The scratch acts as a flaw in the glass and thus determines where the fracture

begins and also influences the direction in which it propagates. Occasionally, longer scratches were made to insure a straight fracture.

A fracture originating in a previously unbroken medium is, for convenience, termed here as an Initial Fracture. When a previously existing fracture is extended it is termed as an Extended Fracture. These two types of fractures are different in many aspects and different techniques have to be employed to produce them. The procedure for producing Initial fractures is, as stated before, by the application of a gas flame about 1.5 cms away from the end of a 0.5 cm long scratch. In the beginning it was assumed that Initial fractures propagate unilaterally, as is observed visually. There was a possibility however, that the Initial fractures might be propagating bilaterally. To resolve the doubt, an experiment was performed. The gas flame was applied at different distances from the edge of the scratch. At a distance of 10 cms there was no fracture formation even after heating for 5 minutes. At a distance of 5 cms, a fracture was observed to form after 4.5 minutes. The fracture remained static for a short while and then propagated both ways. The end moving towards the flame came to a stop after reaching the central heated zone. The heating time required for fracture formation decreased with the distance of the

point of application of flame from the edge of the scratch. The minimum distance and time required for fracture formation was found to be 1.5 cm and 30 secs. The end of the fracture that moves away from the flame usually proceeds a considerable distance (about 10 cms or more) before coming to a stop. It is this end which gives the erroneous visual impression of unilateral propagation. To standardize observations, and to preserve the glass plate for further use, a spot A is heated (fig.9) in addition to spot B. The heating at spot B actually causes the Initial fracture to form, while heating spot A causes the other end of the fracture to stop.

The technique for producing Extended fracture is more involved. As in the case of the Initial fracture, the central zone, with zero or compressive hoop stress is used to stop fracture at a certain point. The central heated zone is also used to lock in sufficient energy. Once a fracture is formed, a large concentration of stress occurs at the tip (the well known $r^{-\frac{1}{2}}$ singularity). Therefore it requires very little energy to extend a pre-existing fracture. Our problem here is to lock in enough energy around the existing fracture which will be released at the time the fracture extends. This is done by heating spot A. The hoop stress set up by heating spot B (fig.10) will then have to overcome the compressive stress at A.

In addition a spot C has to be heated to prevent the fracture from extending indefinitely.

It is also possible to extend the fracture in the direction B D by heating at E. In this case the spot C has to be heated (figure 11), to prevent the fracture from extending in the wrong direction. Of course the spot D has to be heated to prevent the fracture from running away, and the spot B has to be heated to lock in energy. Thus the technique for extending long fractures is different from that of extending short fractures.

Extended fractures are not as sudden as Initial fractures. The passage of the fracture through the zone of compression is slow and proceeds in short spurts. Only after the crossing of the zone of compression does the fracture 'go with a bang'. Extended fractures are always preceded by a number of 'fore shocks'. These are discrete audible 'tinks' which usually do not have enough energy to set off the trigger. The fore shocks' are probably due to some process along the fracture interface, and not at the tip of the fracture.

3.3 Electronic Display and Recording System.

Two different but basically similar electronic circuits have been used. The first system (fig.12) is used for velocity measurements and calibration of detectors.

The second system is used for studying elastic wave radiation from propagating fractures (fig. 13). The first system is essentially the same as that used by Oliver, Press and Ewing (1954), while the second is the modification of the same to fit the special requirements of nonrepetitive nature of individual observations.

The source of elastic energy for the first circuit is a ceramic disc transducer activated by a high voltage short duration pulse from a pulse generator. The pulse generator is triggered by a low frequency (10 - 20 cycles/sec) square wave generator. The detecting part of the circuit consists of ceramic transducers - preamplifier - variable band pass filter - oscilloscope - camera. In addition a trigger take-off circuit amplifies a triggering signal from the pulse generator and triggers the 502 oscilloscope sweep.

The second system is similar to the above except that no preamplifier is used because of the higher energy of elastic waves from fracture. The triggering signal comes from a detector near the expected origin of the fracture. The various components of both the systems are discussed in detail in the following sections.

3.3.1 Ceramic Transducers.

Barium Titanate transducers were used to pick up elastic waves and convert them to electrical signals. Two

types of transducers were used: cylinders and benders. The cylinders are 0.25 cm in thickness and 0.64 cm in diameter, and are mainly sensitive to motion along the axis. The bender consists of two thin strips of barium titanate fused together to form a parallelepiped of dimensions 0.05 x 0.16 x 1.27 cm. They are polarized such that the voltage generated by the two strips add up and increase the sensitivity. The benders are most sensitive to differential displacement perpendicular to the plane of adhesion, and are very direction sensitive. Cylinders can only be used along the edge of a plate to detect P oscillations, while benders can be used on the surface of the plate to detect either P or S waves. If the bender is oriented with flat side along the direction of propagation, mainly S waves are picked up. A change in orientation by 90°, so that flat side is perpendicular to the direction of propagation, means that mainly P waves are detected.

The discs and benders were mounted in low velocity fibre rods to avoid reflections from end of the rods. To further prevent ringing both benders and discs were clamped with foam rubber. The frequency response of the transducers is not known, and can be expected to be non-uniform over the range of frequencies used. To avoid this difficulty, most observations were made in a very narrow

frequency range. Both high and low cut-off dials of the filter were set at the same frequency (10^5 cps); the 3db attenuation point then occurs at 0.77 and 1.30 times the cut-off frequency.

The voltage output of the transducers ranges up to 4 volts at the extreme low frequency range, but is lower at higher frequencies and some amount of amplification is necessary. In the present study the energy of waves radiated from a crack is sufficient to give a transducer output of the order of millivolts. An amplification of 100 is usually sufficient to allow the signal to be properly displayed on the oscilloscope screen.

3.3.2 Filter System.

A filter system is necessary to eliminate external electromagnetic and acoustic noise that is picked up and amplified. Major sources of electromagnetic noise are fluorescent lamps, switches, and normal 60 cycle hum. Acoustic noise is caused by movement in the laboratory, machinery in the building, passing trucks, and occasionally loud conversation.

As discussed earlier, the choice of wave length is rather critical; it must be small enough so that the receiver to source distance is at least several wavelengths. On the other hand the wavelength must be large in

comparison with the plate thickness. In order to fulfil these conditions a frequency close to 10^5 cps is required, both higher and lower frequencies being undesirable.

A commercial variable band pass filter (Kron-Hite 310 AB) was used. The filter consists of several sections of resistance capacitance combinations. The gain between output and input terminals is unity. In any variable band pass filter, some amount of phase distortion is unavoidable. The distortion is zero in the mid-frequency range, gradually increasing as one moves away on both sides of the mid-frequency. When the high and low cut-off are set at the same frequency, the phase distortion is negligible.

A setting of the low-cut-off dial at 2 kc/s effectively eliminates ordinary electromagnetic and acoustic noise. (This is strictly true for a signal amplification of 100; the setting is liable to vary with higher amplification).

3.3.3 Amplifier System.

The high internal gain of the Tektronix 502 oscilloscope makes an external amplifier unnecessary. For calibration and for velocity measurements it is sometimes necessary to detect signals from a pulsed transducer as a source of elastic energy. The energy of waves is low and

amplification of the order of 10^3 is essential. In such a case a commercial battery powered amplifier (Tektronix) or a laboratory designed instrument is used. Both types have suitable amplification and low noise characteristics.

3.3.4 Display and Recording.

The filtered and amplified signal from the transducer is displayed on the screen of a Tektronix 502 or 535 oscilloscope. A DuMont camera with a Polaroid back is used to photograph the display. The camera back is movable, permitting several exposures to be made on the same print.

3.3.5 Triggering System.

To record the disturbances from the fractures special instrumentation was developed. In the usual two-dimensional model seismic experiment (Oliver, Press and Ewing, 1954) a short duration, high voltage pulse is applied to a transducer to provide a source of elastic energy. This pulse also triggers the oscilloscope sweep so that first motions at different points in the medium can be observed. In the present investigations the source of elastic energy is a propagating fracture with unpredictable time of origin. To provide a triggering signal, a detector is placed very near the expected point of origin of the fracture. The detector is a Barium Titanate bender. The signal from the bender is amplified, crudely filtered

of low frequency hums, and fed into the single-sweep circuit of a Tektronix 535 oscilloscope. A gating signal from this oscilloscope is used to trigger the sweep of a Tektronix 502 oscilloscope on which the Polaroid camera is mounted.

Because of the high energy of the elastic waves generated by fractures, acoustic 'noise' persists in the glass plate for times ranging up to tens of milliseconds. This is long compared with the beam sweep time across the oscilloscope screen. To prevent confusion of the first recorded motions with succeeding signals it is imperative that the recording stop after the beam has moved across the oscilloscope screen once. The single sweep circuit of the Tektronix 535 generates one gating signal after receiving the first of a train of triggering signals from the trigger amplifier, and then shuts off until reset. Hence, the beam of Tektronix 502 oscilloscope sweeps across the screen once, until the single sweep circuit is reset.

3.4 Mechanical Arrangement.

Glass plates of dimensions 45 x 45 cms or 60 x 60 cm were used in the experiments. The plates are used commercially as window glass. The cost for the larger plates is approximately 60 cents. No special treatment

was given to the glass plates. The thickness was approximately 3 mm, although plates of other thickness have occasionally been used.

The recording time was too short for an elastic wave to be reflected a sufficient number of times to set up free oscillation of the plate. Therefore elaborate mounting and supporting arrangements for the plate were unnecessary. The plate was supported horizontally by two wooden bars 1.2 cm wide. These were placed along the edges of the glass plate.

The ceramic transducers were mounted in fibre rods and clamped with rubber or foam plastic. The fibre rods are clamped onto movable benches made of steel rods. The coupling between the benches and fibre rods was loose, making the possibility of the whole system ringing remote.

CHAPTER IV

PROCEDURE

4.1 Calibration of Detectors.

The characteristics of each transducer varies significantly with the type of mounting, and with individual ceramic pieces. A procedure has been worked out for choosing from a group of detectors only those which 1) show a response in the 100 kc/s region, 2) exhibit no ringing at that frequency and 3) show definite directional sensitivity to longitudinal and transverse oscillations of the elastic plate. There should be a minimum of pick up of transverse waves when the detector is oriented for longitudinal oscillations, and vice versa.

Without a standard and convenient method of obtaining the frequency response of detectors one can use only an empirical system of cross checking. The principle is simple. Let us define as noise any signal other than a direct P and S wave from a point source (such as a pulsed transducer) on an elastic plate. The direct P and S vibrations are termed signals. If we use a detector with unknown characteristics we will observe in addition to the true signal a considerable amount of noise. If the transducer is improperly damped then a ringing will be observed after the P or S signal is received. As the

exact wave form of the elastic signal at 100 kc/s is unknown, one can compare the signals from two detectors. If they are not similar in form and phase, then one of the detectors is unsuitable. Testing of a large number of transducers will provide a group whose responses are reasonably identical.

The elastic source used in preliminary testing is a pulsed transducer which gives a mechanical impulse to the plate on receiving a 1 kv spike pulse from a pulse generator. The amplitude of the elastic signals received from such a source is small, being about 100 times smaller than those received from fractures. Hence another test is done to determine if the detectors maintain their response at signals of high amplitudes, and are not over-driven. Two detectors are placed at the same position with respect to an Initial fracture. The resulting signals should be identical at least up to 200 micro seconds after the receiving of the first signal.

Instrument Settings - The filter high and low cut-off dials were set at 100 kc/s. The signal amplitude after filtering is around 1 to 10 millivolts. The oscilloscope settings were from 1 mv/cm to 10 mv/cm, and 20 μs/cm.

4.2 Velocity Measurements.

Measurement of P and S wave velocities in glass plates was made using a pulse generator for a source. The circuit for this measurement is given in figure 12. A high voltage (1 kv) spike was applied to a ceramic disc transducer placed at the edge of a glass plate. P and S waves were recorded at 10 cm intervals. The velocity was calculated from the slope of the straight line of the plot of time of arrival against the distance.

An alternative method of measuring the velocity of P and S waves is by placing two detectors about 40 cms apart and recording P and S waves from a fracture. As the elastic disturbance from a fracture is of much higher amplitude it is easier to pick out the desired P or S signals. However, only two detectors can be used for each fracture. Thus, the method is less accurate than the first one and is used only for rough measurements. Moreover, the first method permits an estimate of the error.

4.3 Identification of P and S Waves.

The P phase is the first arrival and its first motion can be picked up with a good deal of confidence. Unfortunately, this is not the case for the S phase which arrives in the midst of spurious pick up of the P phase by the S detector. In order to sort out the first motion

of the S wave it is necessary to study several records and to employ such aids as the calculated arrival time for S waves. After sufficient S signals had been identified it was noticed that the S waveform was quite similar to the P waveform in the frequency range investigated. Thus an additional check upon the identification of the first S motion could be obtained by matching peaks and troughs of the P and S waves.

4.4 Determination of the Radiation Pattern.

The non-repetitive nature of each observation controlled the experimental procedure. Ideally, to observe the radiation pattern from a source like a fracture, one should have a battery of identical instruments surrounding the source. However, for this series of experiments only two recording channels were available. Moreover, the variation of the coupling of individual detectors to the glass makes it seem unlikely that more than two channels could be used successfully.

The energy released by each fracture is extremely variable. So for the direct plotting of either the P or S radiation pattern a monitoring detector is necessary. This monitor is placed at a fixed distance and at a fixed angle with respect to the fracture. The other detector is placed at various angles θ with respect to the fracture.

The measured amplitudes are normalized with respect to the monitor. The coordinate system, as defined before, is as follows: the fracture propagates in the positive X direction; the direction normal to the fracture, in the plane of the plate, is Z. The origin of the cartesian system is also the origin of the polar system. Angle Θ is measured in an anticlockwise manner from the positive X axis. In the polar system we define (following Knopoff and Gilbert) outward radial motion as positive, and anticlockwise tangential motion as positive, on the X - Z plane. Figure 4 shows the details of the coordinate system and the direction of positive unit vectors.

The amplitude of P waves at Θ azimuth is expressed as a non-dimensional ratio with respect to amplitude of P at 90°. For S waves the S_{Θ}/P_{Θ} amplitude ratio has been determined at various azimuths. Knowing the P_{Θ}/P_{90} ratio at the particular azimuth it is possible to determine S_{Θ}/P_{90} for any Θ .

A major problem has been the variable contact between the glass plate and the two measuring transducers. Without any compensation for such unequal coupling, a large scatter in the values of P_{Θ}/P_{90} and S_{Θ}/P_{Θ} ratios was observed. A method has been devised which eliminates the effect of unequal coupling. Let two transducers be designated A and B. First A is used for recording P_{Θ} ,

and B for recording P_{90}, from a fracture F_1. Next, without disturbing A or B, a different fracture location F_2 is used so that A now records P_{90}, and B records P_Θ. This constitutes a set of readings. The ratios are

$$P_\theta(A) / P_{90}(B) \qquad \text{and} \qquad P_\theta(B) / P_{90}(A)$$

The mean

$$\frac{1}{2}\left[P_\theta(A) / P_{90}(B) + P_\theta(B) / P_{90}(A) \right] = P_\theta / P_{90}$$

is now independent of unequal coupling at the contacts of transducers A and B and the glass plate. Each measured ratio, therefore, represents the mean of two observations from two different fractures. The arrangement is shown in figure 14. Transducers A and B are oriented so as to record only the $\cos\psi$ component of P radiation. The ratio of course is independent of ψ. The angles θ, ψ and the separations r, f, and d are shown in the figure. The distance r between the fracture origin and the transducers is 30 cms.

From geometry

$$\angle F_1CD = \angle CF_1A + \angle CAF_1$$

or $$\pi/2 - \psi = \theta + \psi$$

or $$2\psi = \pi/2 - \theta$$

therefore $$\psi = \pi/4 - \theta/2$$

and $$f = r \sin \psi$$

and $$d = r \cos \psi$$

The quantities ψ , d and f are calculated for r = 30 cms and different θ and are shown in Table 1.

As the S amplitude is small at 90°, the same arrangement cannot be used for S wave measurements. Besides the orientation of the transducers at an angle to the line joining the point of observation to the fracture origin would cause a significant amount of pick up of P waves which will interfere with S wave observation. However, if we study the S_θ / P_θ ratio then the interchange of transducers is again possible. Designating the transducers as A and B, as before, we use A to record P_θ and B to record S_θ , from the fracture F_1. Next <u>without disturbing A or B</u>, a different fracture location F_2 is used so that A records S_θ and B records P_θ . We have the ratios

$$S_\theta(B) / P_\theta(A) \qquad \text{and} \qquad S_\theta(A) / P_\theta(B)$$

The mean gives S_θ / P_θ , which is independent of unequal coupling. The arrangement for this is shown in figure 15. The separation r is equal to 25 cms.

4.5 Determination of the Far - Field Region.

The first motion theory of Knopoff and Gilbert is valid only in the far field region, i.e., a sufficiently

large number of wavelengths away from the source. It was considered necessary therefore to determine whether the distances of 25 and 30 cms from the source are indeed within the far field region for P waves with wavelengths of 5.5 cm. Because of the geometric spreading of energy the amplitude of two-dimensional waves is proportional to $r^{-\frac{1}{2}}$ in the far field region. Here r is the distance of the point of observation from the source. In the near field region the value of the attenuation constant is higher.

As before, the arrangement involved interchange of transducers A and B to eliminate the effect of unequal coupling. Transducer A is first used to record P_{90} at 20 cms,and B is used to record P_{90} at r cms distance from fracture F_1. Next, without disturbing either A or B, a new fracture location F_2 is used such that A now records P_{90} at r cms and B records P_{90} at 20 cms. The arrangement is shown in figure 16. Let us assume the amplitude is proportional to r^n. Then, normalizing our results to 20 cms we have the ratios

$$\frac{P_{90}(r)}{P_{90}(20)} = \left[\frac{P_{90}(r)(B)}{P_{90}(20)(A)} + \frac{P_{90}(r)(A)}{P_{90}(20)(B)}\right] = \left[\frac{r}{20}\right]^n$$

or $$\ln\left[\frac{P_{90}(r)}{P_{90}(20)}\right] = n \ln\left[\frac{r}{20}\right]$$

A least square analysis gave the value of n to be

$$-0.53 \pm 0.08 \text{ (standard error)}$$

The points are plotted on log log scale in figure 17. The value of n indicates that the region $r \rangle 20$ cms is definitely within the far field region.

A similar study, with identical arrangement, was made for P_0 . The value for n in this case came to be

$$-0.45 \pm 0.09 \text{ (standard error)}$$

This confirms the previous measurements. The data is plotted on log log scale in figure 18.

4.6 Symmetry of Initial Fractures.

As mentioned in section 3.2, a test determined that Initial fractures are bilateral in nature. The fracture is initiated by inducing thermal stress mostly at one end (figure 9). The other end is heated only to stop the fracture from propagating too far. Therefore we had reason to suspect that there might be an unequal radiation between the A and the B sides. We tested for symmetry by simultaneously measuring amplitudes at 45^{o}

and 135° S waves from Initial fractures. The rough measurements of the ratio of S_{135}/S_{45} came to be 0.96 ± 0.08 (standard deviation of the mean). Therefore we find no evidence of bilateral asymmetry of Initial fractures induced by our method.

CHAPTER V

RESULTS

5.1 General.

Energy from Initial and Extended fractures ranges from the audio into the 200 kc/s region. The eigenfrequency of the glass plates did not permit us to observe and record the audio frequencies. But each fracture is signalled by a clearly audible 'ping', indicating measurable energy in the audio range. There is some relationship between the sharpness of the 'ping' sound and energy content in the high frequency 100 kc/s region. Fractures with 'pings' of high audio frequencies usually show higher amplitudes in the 100 kc/s region. Almost all fractures that produced very loud, but low audio frequency noise ('bangs') showed no appreciable amplitude in the 100 kc/s region.

The P 'waveform' observed is produced by eliminating all of the signal except a narrow frequency band around the 100 kc/s region. It is remarkable therefore to observe the reproducibility of the 'waveform'. The usual P waveform consists of three extrema, two peaks and a trough. All first motion measurements have been made by a) measuring the height of the first extremum, or b) measuring the vertical separation between the first and the

second extrema. The procedure (b) has been used only when the first extremum is very small or when (as for S waves) the exact arrival is indistinct. The signal to noise ratio is higher if procedure (b) is employed, and the errors of measurement are less.

Measurements of the first S motion have not been so easy. It is not too difficult to find the S wave, but difficulty is experienced in the identification of first S motion. The exact beginning of S is obscured by pick up of spurious P oscillations of variable amplitude. It appears that the S waveform at 100 kc/s resembles the P waveform at this frequency. Then the identification of first S motion is simply a question of looking for the three extrema characteristic waveform of P wave. The first S motion, then, is the first of three extrema. If the S waveform is different from the P waveform by having a small first motion preceding the three extrema, then the first S motion is extremely difficult to identify and measure. If such is indeed the case, our measurements, based on the three extrema waveform, will be altered in magnitude as well as sign. Such a possibility is unlikely, as can be seen from some typical P and S three extrema waveform shown in figures 19 and 20. Definite arrival of S waves can be identified by the kinks that appear in some traces. The usual three extrema waveform follows the kinks. However,

all S arrivals are not so definite and clear, giving rise to the ambiguity of first motion. We mention this here because the sense of the observed first S motion is opposite to that predicted by Knopoff and Gilbert.

The ratios P_θ / P_{90} and S_θ / P_θ have been measured for various θ for both Initial and Extended fractures. The S radiation pattern can be determined from

$$S_\theta / P_{90} = P_\theta / P_{90} \times S_\theta / P_\theta$$

The errors being compounded are much higher than for either P_θ / P_{90} or S_θ / P_θ. However, we could find no direct means of determining S_θ / P_{90} ratio which would also permit us to interchange transducers to eliminate the effect of unequal coupling. Scatter is observed in successive measurements of the ratios at the same θ. We use the standard deviation for an individual observation, and the standard deviation of the mean as measure of scatter. The following definitions of these quantities have been used

Mean $$\bar{x} = \frac{\sum x_i}{n}$$

Standard Deviation $$\sigma = \left[\frac{| x_i - \bar{x} |^2}{n-1} \right]^{1/2}$$

Standard Deviation of the mean $$\sigma_\mu = \frac{\sigma}{\sqrt{n}}$$

where x_i represents the n values of P_θ / P_{90} or S_θ / P_θ at the same θ . In general the standard deviation ranged 10 to 20 per cent of the mean. The standard deviation of the mean is of course much lower.

The data is presented in Tables II to VII and Figures 23 to 26. Theoretical values at each azimuth are given for comparison.

5.2 Initial Fractures.

The measured P_θ / P_{90} and S_θ / P_θ ratios are shown plotted in figures 23 and 24 and tables II and III. The standard deviation of the mean is also plotted as vertical lines as a measure of uncertainty. . The theoretical curves, calculated from the formulae of Knopoff and Gilbert are shown for comparison. For P_θ / P_{90} the agreement is good for $30^\circ < \theta < 90^\circ$. In the $\theta < 30^\circ$ range the observed P_θ / P_{90} is almost constant in value. The S_θ / P_θ measurements show reasonable agreement with theory in magnitude up to $\theta = 45^\circ$. For $\theta < 45^\circ$ the measured magnitudes are smaller. The sense of S motion is opposite that predicted by theory. Considering the disagreement in both P_θ / P_{90} ratio and the S_θ / P_θ ratio we can conclude that the S_θ / P_{90} ratios will differ from the theoretical values in the $\theta < 45^\circ$ range.

5.3 Extended Fractures.

We believe that Extended fractures are unilateral dislocations of the type described by Knopoff and Gilbert as their model III. If so, then the measured ratios of P_Θ/P_{90} and S_Θ/P_Θ differed markedly from theory. There is no reversal of direction of motion at P_O with respect to P_{90}, as predicted by theory. All measured ratios of P_Θ/P_{90} are positive, indicating motion away from the source. By theory, the motion should be towards the source in the $\Theta < 25^\circ$ region. The measured P_Θ/P_{90} maxima falls in the forward quadrant instead of around $\Theta = 100^\circ$. Therefore, except for $\Theta = 90^\circ$, the normalizing point, the measured values do not agree with theoretical values. Referring to figure 26, we see that the S_Θ/P_Θ ratio also shows lack of agreement with theory. As P amplitude does not go to zero or become negative in the first quadrant, there is no singularity in the measured value of S_Θ/P_Θ in the first quadrant. As in the Initial fracture, the sense of S motion is opposite that given by theory.

Several difficulties were encountered in measurements from the Extended fractures. Firstly the amplitudes of waves was 2 - 5 times lower than the amplitude of waves from Initial fractures. Therefore measurements had greater scatter, due to the decreasing signal to noise ratio. The second difficulty was that Extended fractures

tended to creep a short distance before going with a 'bang', as it were. The result was that both P and S waves were emergent, and not sharp. In the $90^{\circ} < \theta < 180^{\circ}$ quadrant the frequency was about half of the frequency in the forward quadrant, in spite of the narrow filter bandwidth (figure 22). The measurements in the back quadrant therefore are of dubious value. This is particularly true of S_{θ}/P_{θ} measurements. We have not presented any data for S_{θ}/P_{θ} measurements in the $90^{\circ} < \theta < 180^{\circ}$ region.

CHAPTER VI

DISCUSSION

6.1 General.

From the results presented in the last chapter it can be realized that our measured values differ considerably from those of Knopoff and Gilbert. The disagreement could be due to various factors, the major ones being whether our model corresponds to the type of dislocation contemplated by Knopoff and Gilbert in their Model 3 dislocation, and whether we have taken care to satisfy the various assumptions in the theory. From the determination of the attenuation factor, we can be confident that our measurements have been made in the far field region, as envisaged in the theory. The Initial Fracture definitely corresponds to Model 3 of Knopoff and Gilbert for bilateral propagation. The Extended Fracture should correspond to the unilateral propagation of a discontinuity in the difference of u_z. But we can only state with certainty that the fracture propagates only one way, while there might be a bilateral propagation of dislocation. However, from our measurements it appears that most of P and S energy is radiated in the forward direction from Extended Fractures. The extreme asymmetry makes the possibility of a bilateral dislocation

propagation from a unilateral fracture unlikely.

6.2 High Frequency.

The theory of Knopoff and Gilbert is only valid for first motions, i.e. the high frequency solutions. But they have not given any criterion for determining whether a certain frequency is sufficiently high. Therefore we are forced to use our own interpretation of what is high frequency. A most empirical criterion, valid for static sources, is that the frequency is high if the wavelength is much smaller than the source dimensions. In the present case the theory assumes a propagating point source. Hence any arbitrary wavelength can be shown to be longer than the source dimension, and this criterion has no meaning. The interpretation of first motion is further complicated by the fact that the theory assumes an ideal step-function displacement at the source. In the case of the actual fracture the displacement probably returns to zero after a short time. Our criterion for high frequency is as follows. Let τ be the time over which first motion amplitude measurements are made on a signal. In our usage τ would mean the time interval between arrival of the signal (P or S wave) and the second extrema. In figure 27 OO'B is the direction of fracture propagation and A is the point of observation. In the interval the tip of fracture

moves from O to O', where $OO' = \delta\gamma$. The angle AOB is θ and the angle AO'B is $\theta + \delta\theta$. We contend that γ is sufficiently small if the angle $\delta\theta$ is negligibly small. In the present case

$$\delta\theta = \frac{\delta\gamma}{r} = \frac{2}{30} = 3^\circ 50'$$

This $\delta\theta$ is an outer limit and constitutes a small fraction of the total θ. If the time range is considered a rough measure of the time period of the high frequency, we get the corresponding frequency as 100 kc/s.

6.3 Diffraction Effects.

The P_θ / P_{90} ratio shows marked disagreement with theory only in the $\theta < 30^\circ$ range. This could be due to refraction through the hot spots or diffraction at the edges of the fractures. The effect of hot spot has been shown to be small in section 3.3. The refraction effects due to the hot spot could not be significant as the elastic properties of this type of glass change only 3 per cent over the temperature range of 0° to 200°C. To determine if the disagreement is due to the diffraction at the edges, we measured the attenuation constant for P at $\theta = 0^\circ$. The procedure and experimental set up is similar to that described in section 4.5. The least squares determination of the exponent of r gave the value

0.45 ± 0.09 (standard error).

This is equal to the attenuation constant for P measured at $\Theta = 90^{\circ}$, within the limits of error. Had the anomalous value of P_{Θ}/P_{90} for $\Theta < 30^{\circ}$ been due to diffraction at the edges the attenuation would differ significantly from 1/2. We can conclude therefore, that diffraction plays no significant role in the measured value of P_{Θ}/P_{90} and S_{Θ}/P_{Θ} ratios.

6.4 Correspondence of Fractures to Other Dislocation Models

We have so far assumed that the fractures induced by thermal stress in glass plates correspond to Model 3 of Knopoff and Gilbert. It is possible that the fractures studied correspond instead to a combination of Model 3 and one or more of the other models. The theory states that there must be a suddenly applied <u>difference</u> in the strain or displacement components on both sides of the fracture plane. A discontinuity in the difference of u would correspond to Knopoff and Gilbert's Model 3. The symmetry of conditions on both sides of fracture plane precludes a difference in the other components of displacement. The same applies to strain components. Any asymmetry that exists is due to random inhomogeneity in the glass and would be one of the reasons for the observed scatter in the measured ratios. We fail to see the possibility of a discontinuity in the difference of any other

strain or displacement component.

6.5 Velocity of Fracture Propagation.

In section 2.2 we contend that the velocity of propagation of fracture is a constant with a value of $0.5\,\beta$. This is the maximum measured value. Fractures have been observed to move at slower velocities, but we contend that this could be the apparent velocity due to the fact that the fracture propagates in short spurts. We must examine the consequences of our assumption being incorrect in that the value of ζ can range anywhere from 0 to α. For $\zeta \to 0$, the term involving ζ in

$$u_p = \frac{\tilde{r}_1}{4\pi r}\left\{\frac{1}{\alpha} + \frac{(2\beta^2-\alpha^2)\cos\theta}{\alpha^2\zeta} - \frac{2\beta^2\cos^2\theta}{\alpha^3}\right\}$$

is preponderant. The ratio $P_\theta/P_{90} \to \infty$ for all θ except $\theta \to 90^\circ$. Obviously this is not the right solution. The expression for u_s is

$$u_s = \frac{\tilde{\theta}_x}{4\pi r}\left\{-\frac{\sin 2\theta}{\beta} - \frac{(\alpha^2-2\beta^2)\sin\theta}{\beta^2\zeta}\right\}$$

Here again the term involving ζ is preponderant for $\zeta \to 0^\circ$. The ratio S_θ/P_θ will then vary as $\tan\theta$. Thus S_θ/P_θ ratio will have a singularity around $\theta \to 90^\circ$, contrary to our measurements.

There is a possibility that the velocity of propagation of fracture may momentarily reach the value of the longitudinal wave velocity. If so, the P_θ / P_{90} curve for $\varsigma = \alpha$ will fall between the curves for $\varsigma = \beta/2$ and $\varsigma = \infty$. It can be seen that the P_θ / P_{90} curve still is a very poor fit for the measured points for Extended fractures, even with $\varsigma = \alpha$.

6.6 Non-linear Effects.

The theory of Knopoff and Gilbert assumes that linear elasticity theory is applicable in the region immediately adjacent to the fracture. There is evidence to doubt this. Firstly the existence of the well-known $r^{-\frac{1}{2}}$ singularity in the concentration of stress at the tip of a crack strongly suggests the possibility of a plastic yield zone in the immediate neighbourhood of the tip of the crack. Secondly experimental photographs presented in Schardin (1959) show a set of propagating fractures with 'coronas' at the tip. In the same photographs there is also a set of static fractures, but in these the coronas are absent. The corona is indicative of a plastic zone at the tip. The radiation pattern from a propagating fracture would therefore be complicated by the zone of plasticity. It is conceivable that the initial disturbance is a plastic wave which is converted into an elastic wave some distance

from the fracture. We are certain that our measurements are in the far field region of the source, where linear elastic theory is applicable. But we have no idea of the extent to which the an-elastic zone affects our measurements. It is possible that the disagreement between our measurements and the theory of Knopoff and Gilbert could be explained by taking into consideration the an-elastic effects in the neighbourhood of the fracture.

6.7 Actual Correspondence of Fracture in Plate to Fracture in Three Dimensions.

In section 1.3 we mentioned that on the X - Z plane the first motion comes from an infinitesimal part of the fracture front. In actual case the length of the section is not infinitesimal, and we shall now discuss the effect of finite length on our measurements. Figure 28 shows the infinite fault front propagating in the X direction and extending to infinity along the Y direction. Because of symmetry, we shall only discuss the positive Y direction. The plane of measurement (which in our case is the plane of the plate) is X - Z. The point of observation is A, and OA makes angle θ with the X axis. AC and AD are projections of AO on the X and Z axes respectively. During the time of measurement (τ) of first motion at A, only the element OO' contributes to the

first motion at A. Hence for P waves,

$$- \quad AO'/\alpha - AO/\alpha = \tau$$

Now $$(AO' - AO) = \tau\alpha$$

In our case $$\tau = 5\mu s$$

$$\alpha = 5500 \text{ m/s}$$

$$AO = 30 \text{ cms.}$$

Therefore, $\alpha\tau = 2.75$ cms.

and $OO' = (AO'^2 - AO^2)^{\frac{1}{2}} = (33^2 - 30^2)^{\frac{1}{2}} = 13.7$ cms.

By the argument presented in section 1.3 our measurements, though made on a plate 3 mm thick, are equivalent to signals from a part of the fault front 28 cm long, which is certainly not infinitesimal. At first sight it appears as if all our measurements are invalid. This is not so. Referring to formula (2 - 22) we see that the only factors that could affect the amplitudes of P (or S) are changes in γ_1, γ_2 and r. We can neglect the change in length r, because the attenuation depends on $r^{-\frac{1}{2}}$, which is small. We have to determine γ_1 and γ_2 for AO', with respect to a new coordinate system at O'. Defining these as γ_1' and γ_2' we have, from the figure 28

$$\gamma_x' = \frac{OC}{AO'} = \frac{OC}{AO} \times \frac{AO}{AO'} = \gamma_x \frac{30}{33}$$

$$\gamma_z' = \frac{OD}{AO'} = \frac{OD}{AO} \times \frac{AO}{AO'} = \gamma_z \frac{30}{33}$$

Thus the end of the contributing segment of the fault front has a direction cosine differing from that of AO by 9 per cent. This is large: but it must be remembered that the signals from the end of the contributing segment of the fault front arrive at the tail end of the time of measurement τ and have a relatively minor effect on the first motion. Therefore in the actual case the error is much lower. The P_θ / P_{90} ratio for 0° from Extended Fractures gives theoretical value of 0.01, when the direction cosines in the formula (2 - 22) are reduced by 9 per cent. It still differs considerably from the measured ratio of 0.56. The effect of summation of the contribution of the whole segment will be small. The value for τ for S wave measurements is 10 μs , and similar calculations can be done.

In earthquake seismology, the time period of elastic waves is of the order of 1 second. This corresponds to our period of the order of 10 μs. The scaling factor is thus 10^5. Therefore, 1 cm on the model corresponds to 1 km in the field. Our results, then, are equivalent to

recording on the surface at 30 km distance from a fault 26 km deep. During the time of recording of first motion the fault advances about 3 km. We realize that 30 km is too close to the source, specially in earthquake seismology: but as we have recorded in the far field our results should be valid over much longer distances, at least up to 100 km.

Another interesting interpretation of our results is possible. The contributing segment 00', (Fig. 28) elongates with time at infinite velocity. Instead of considering the tip of the fracture in the X-Z plane as the moving source, it is possible to consider the tip of the contributing segment in the Y Z plane as the moving source. The propagation of the fracture in the plate, then, simply means that the source is widening with increasing τ . The rate of fracture propagation is small compared with the velocity of elongation of the contributing segment. An interchange of coordinates is now necessary. Referring to figures 2 and 28, we now consider the direction of elongation of the contributing segment 0'00'' as the X direction, and the plane of the plate as the Y-Z plane. The fracture in the plate now propagates in the Y direction. Our results can be reinterpreted as measurements of the first motion on the Y-Z plane from a discontinuity in u_z, propagating at infinite velocity in the X direction. The theoretical expressions for u_p and u_s are unchanged if we take $\gamma = \infty$

and measure θ from the Y axis. The curves for P_θ / P_{90} and S_θ / P_θ are the same as shown in figures 23 to 26, except that they now represent values on the Y-Z plane. The effect of widening source (due to the propagation of fracture in the plate, now in the Y-Z plane) will be small. However, even with this interpretation, our measurements still show considerable discrepancy with the theory.

CONCLUSIONS

We have studied the longitudinal and transverse elastic wave radiation in the 100 kc/s range from propagating tensile fractures in glass plates. For Initial (Bilateral) Fractures the P radiation is a maximum in a direction normal to the fracture; the P wave amplitude drops steadily until $\theta = 30^{\circ}$, after which the amplitude is reasonably constant at about 35 per cent of the P amplitude at 90°. For Extended (Unilateral) Fractures, the P amplitude maxima is in the forward quadrant; the P wave amplitude for $\theta = 0^{\circ}$ (in the direction of propagation) is high, being about half the P amplitude at 90°. In all cases the first P motion is away from the source. For S waves, the first motion is away from the fracture plane, towards the normal to the fracture. The experiment essentially constitutes a partial test of the First Motion Theory of Knopoff and Gilbert (1960), for their Case 3. For Initial Fractures the measured first P motion amplitude differs from the theoretical value in magnitude only for $\theta < 30^{\circ}$ range. For Extended Fractures the measured magnitudes differ from the predicted values at all points, except $\theta = 90^{\circ}$. For S waves, the most significant difference is in the sense of the first motion. The measured first S motion

has a sense opposite that predicted by theory. We suspect that the discrepancy between the experiment and theory may be due to the neglect of the non-linear elastic effects at the source of the disturbance (i.e. the fracture tip).

It is impossible to make a precise comparison of experiment and theory since the duration of what is described as first motion in the theory is not precisely defined. Nevertheless, it seems likely that the discrepancies between the experiment and theory described above are real differences in what seismologists would call first motions. If this is so, we conclude that the theory is not adequate to describe all the observations. Although we have tested only one particular case out of eight independent dislocation models proposed by Knopoff and Gilbert, we feel the discrepancies are so serious as to cast doubt upon the usefulness of the theory in other cases.

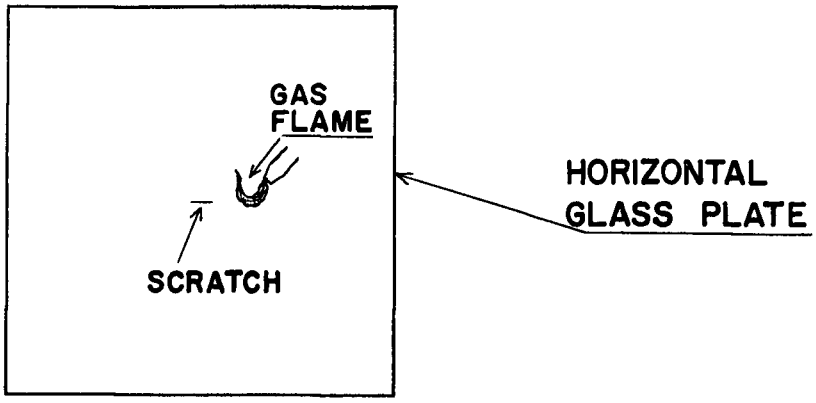

Fig. 1. Method of applying gas flame to glass plate. The glass plate is horizontal.

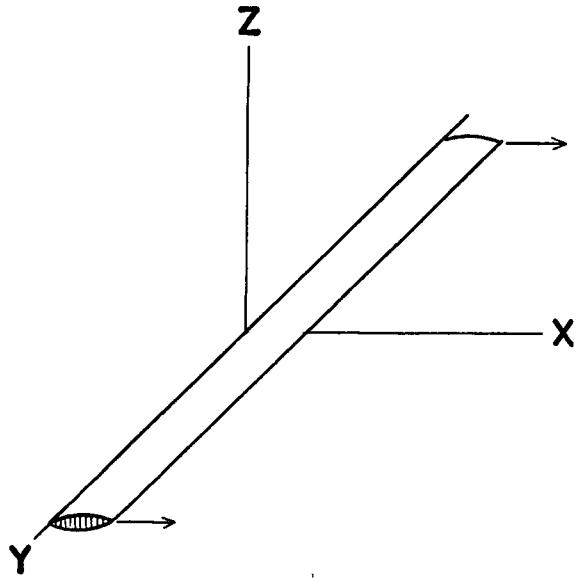

Fig. 2. Infinitely long fracture in three-dimensional body. The fracture front is parallel to the Y axis and propagates in the X direction. The displacement is in the Z direction.

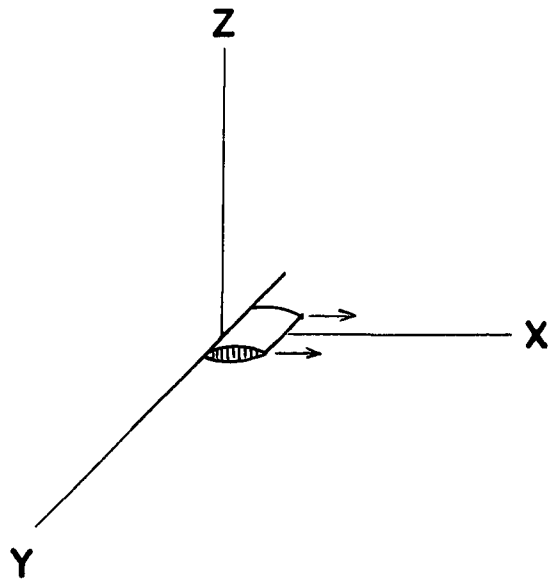

Fig. 3. Infinitesimal part of fracture that contributes to first motion at any point on the X - Z plane.

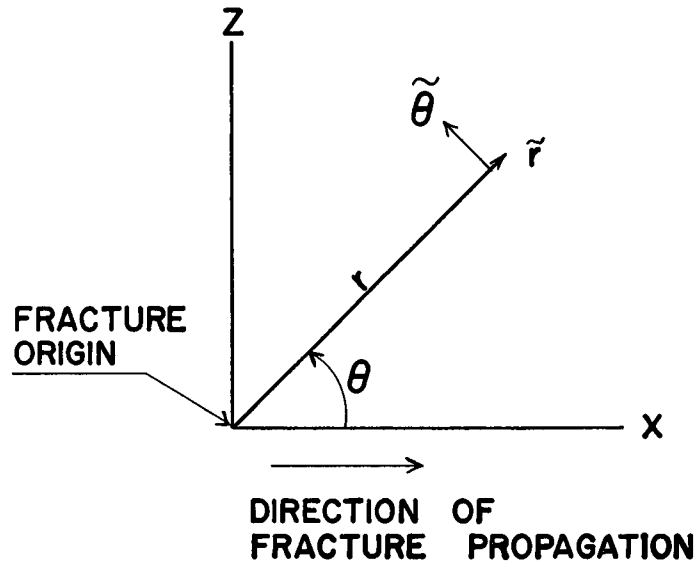

Fig. 4. Coordinate system and direction of positive unit vectors.

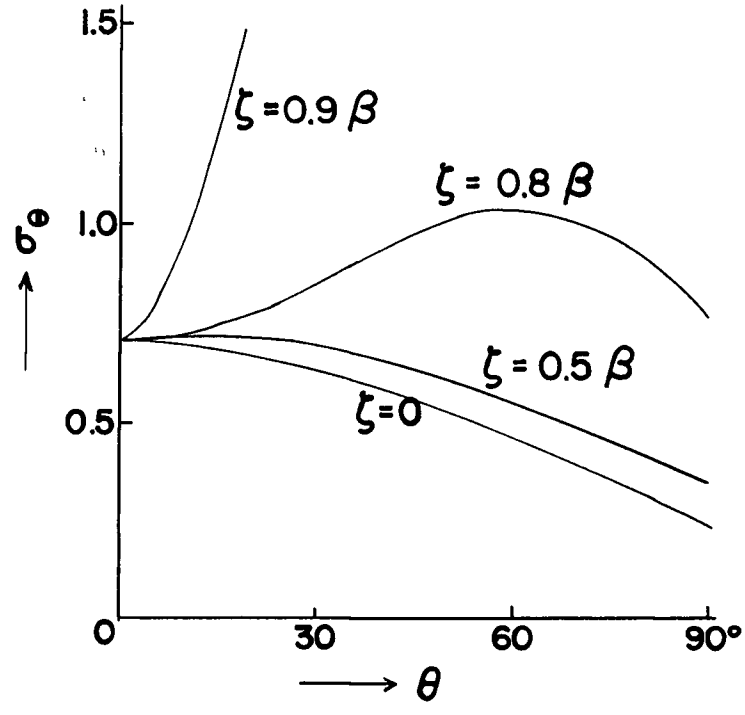

Fig. 5. Distribution of σ_θ with Θ (after Joffe,1951).

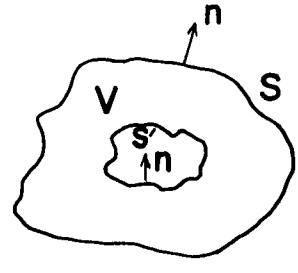

Fig. 6. Figure shows volume V bounded by surfaces S'. The positive normal n to S' is outward. In the limiting case the outer S' goes to infinity and the inner surface shrinks to the fault surface.

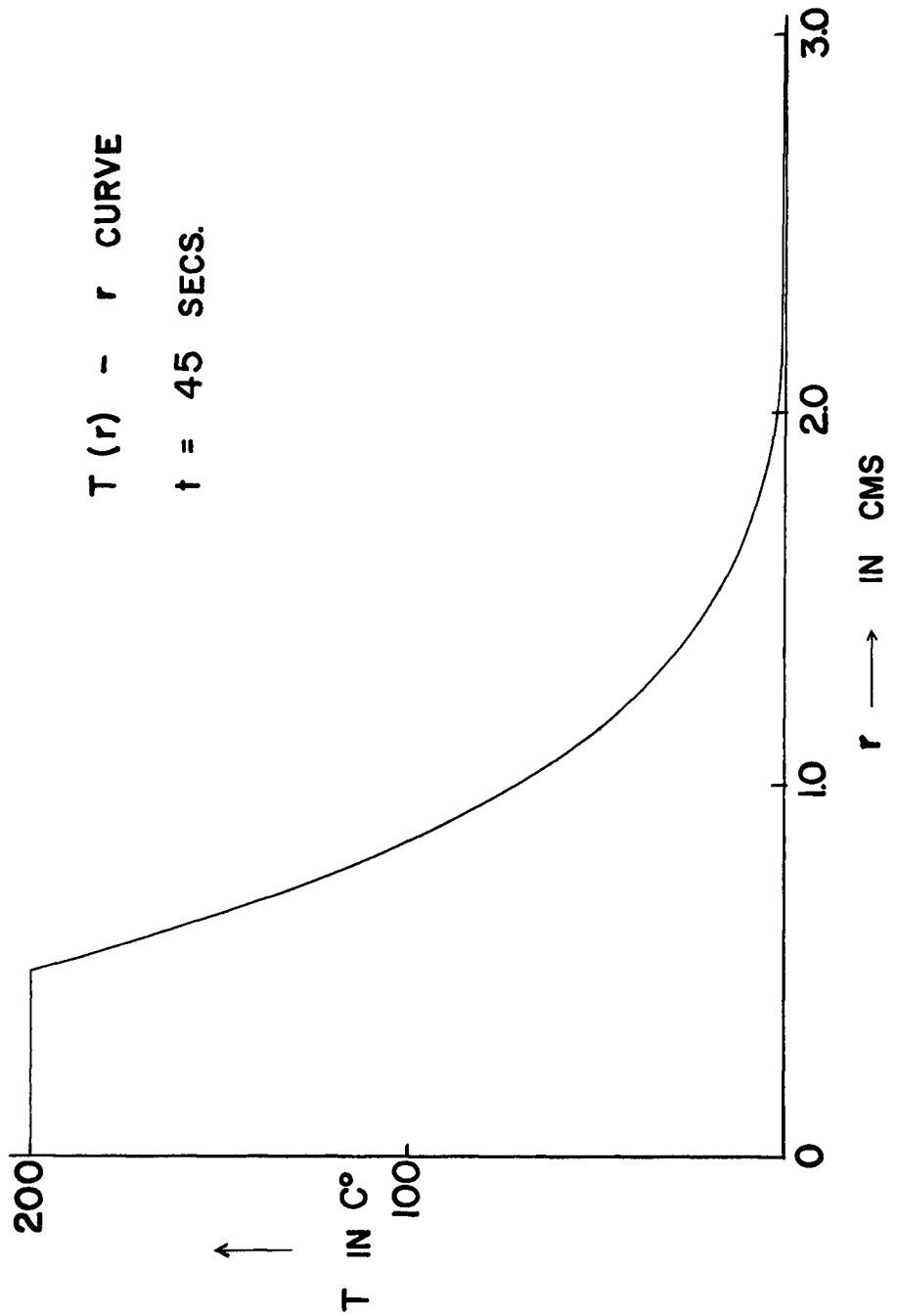

Fig. 7. Distribution of temperature with radial distance on a glass plate. The central region of 0.5 cm radius is suddenly raised to a temperature of 200° C at time t = 0. The figure shows temperature distribution after 45 seconds.

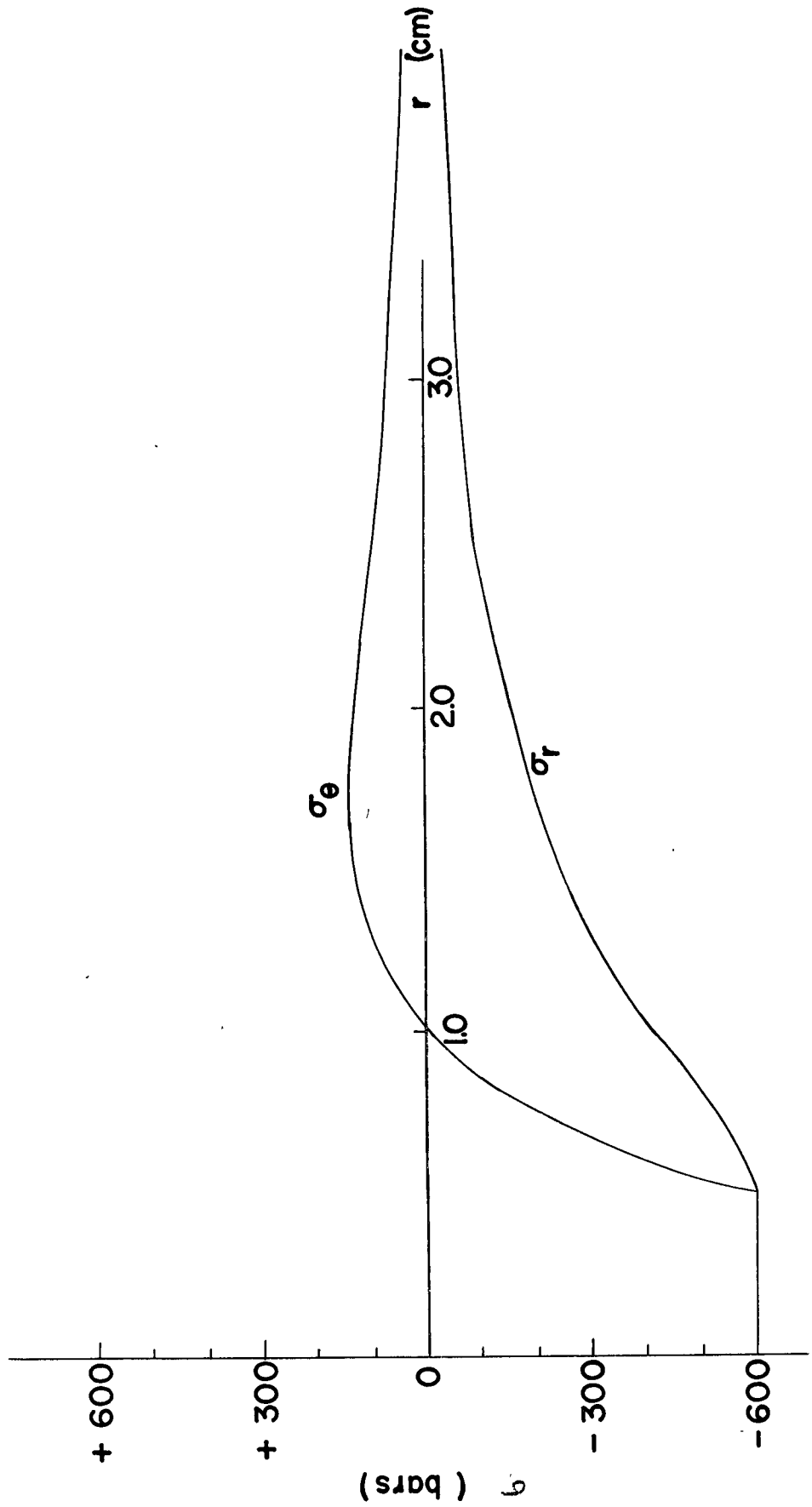

Fig. 8. Stress distribution in the glass plate because of the temperature distribution shown in figure 7.

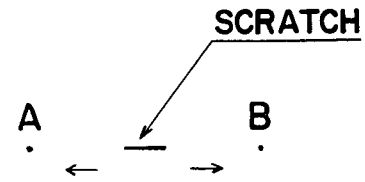

Fig. 9. Method of inducing Initial Fractures. The average length of Initial Fractures is 3 cms.

Fig. 10. Method of extending short fractures.

Fig. 11. Method of extending long fractures.

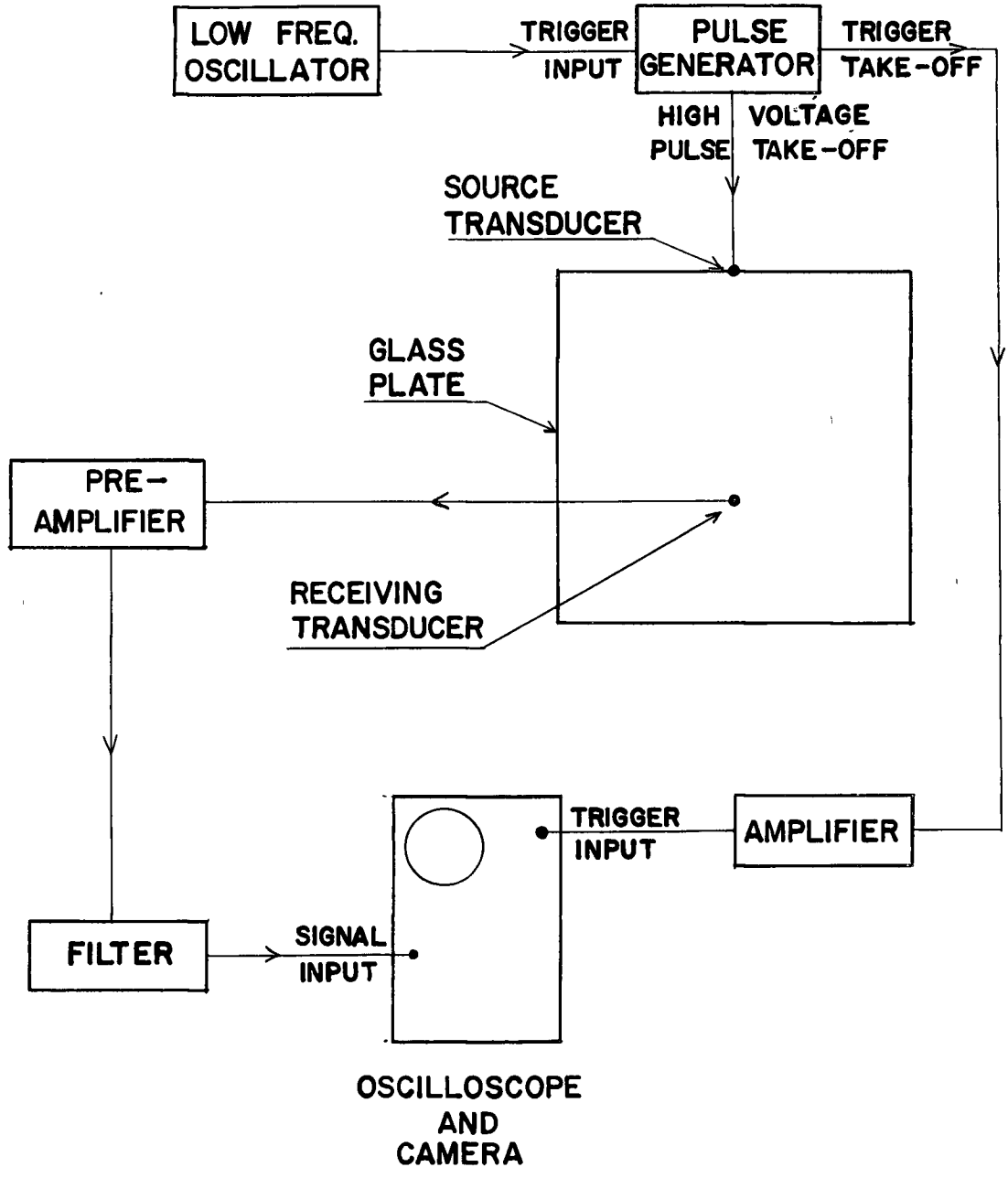

Fig. 12. Schematic circuit for measuring P and S wave velocities in glass plates.

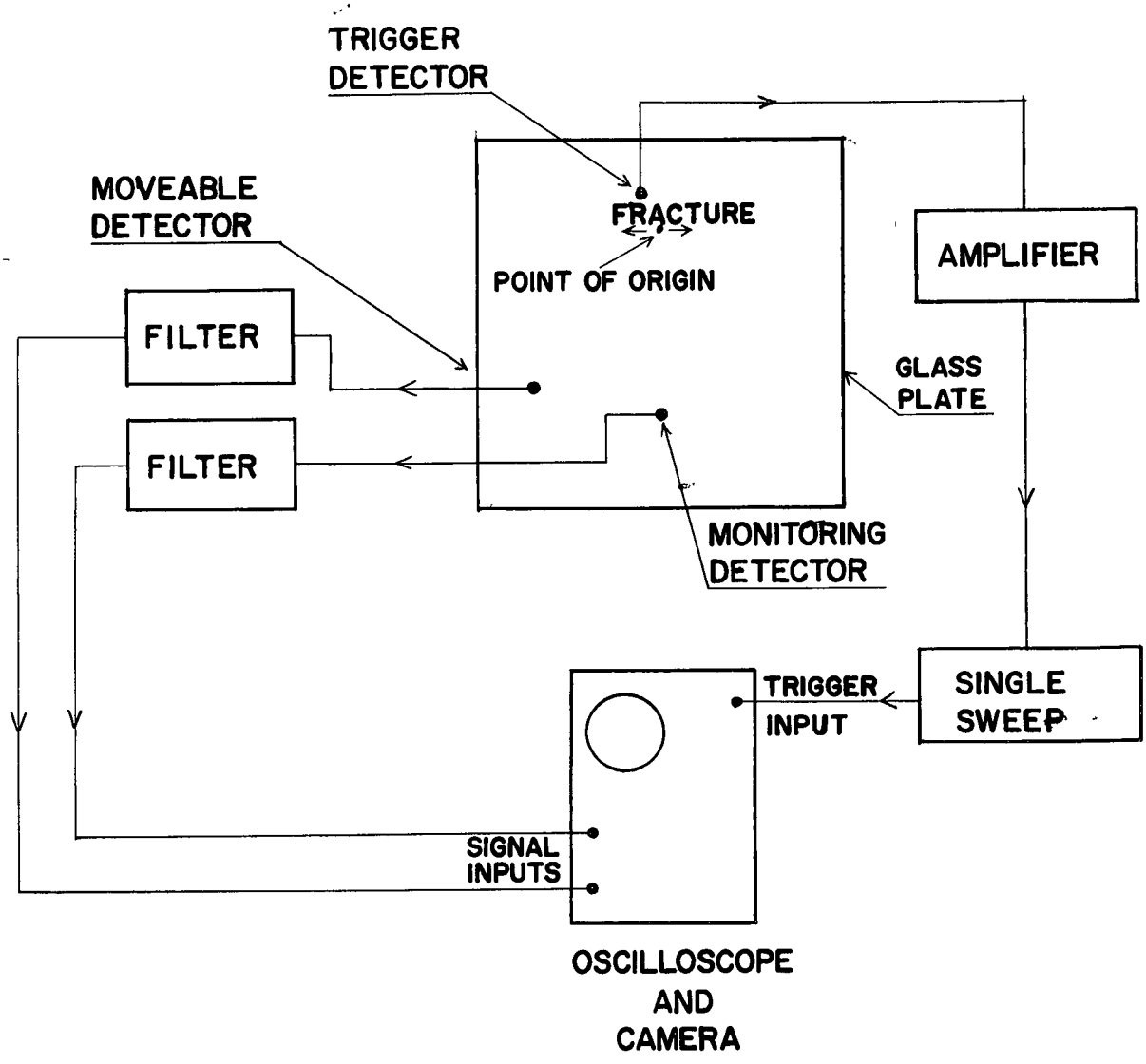

Fig. 13. Schematic circuit for studying radiation from fractures in glass plates.

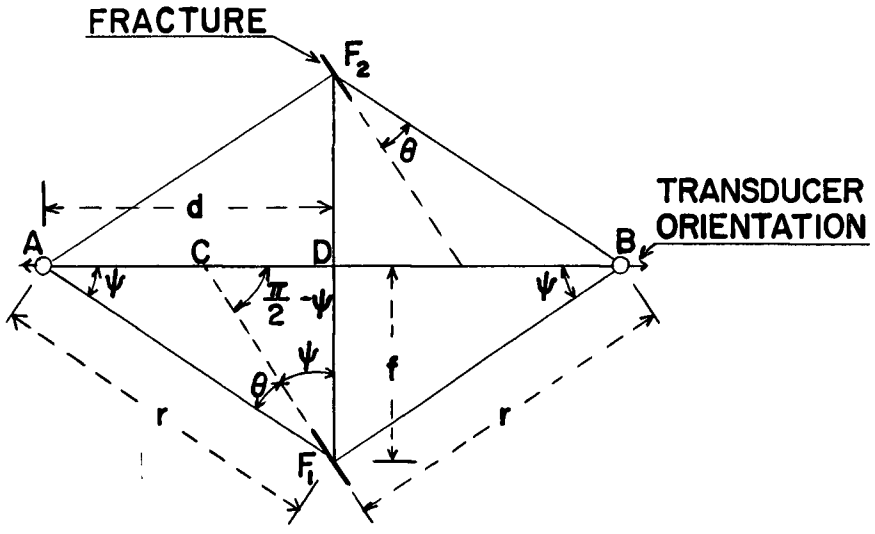

Fig. 14. Transducer and fracture positions for determination of P_θ / P_{90} ratio. Displacement in the direction of arrows at A and B causes upward swing of oscilloscope trace.

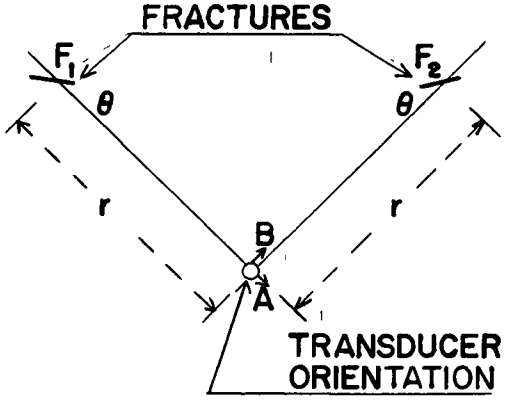

Fig. 15. Transducer and fracture positions for determination of S_θ / P_θ ratio. The angle θ may be replaced with $2\pi - \theta$ for small θ.

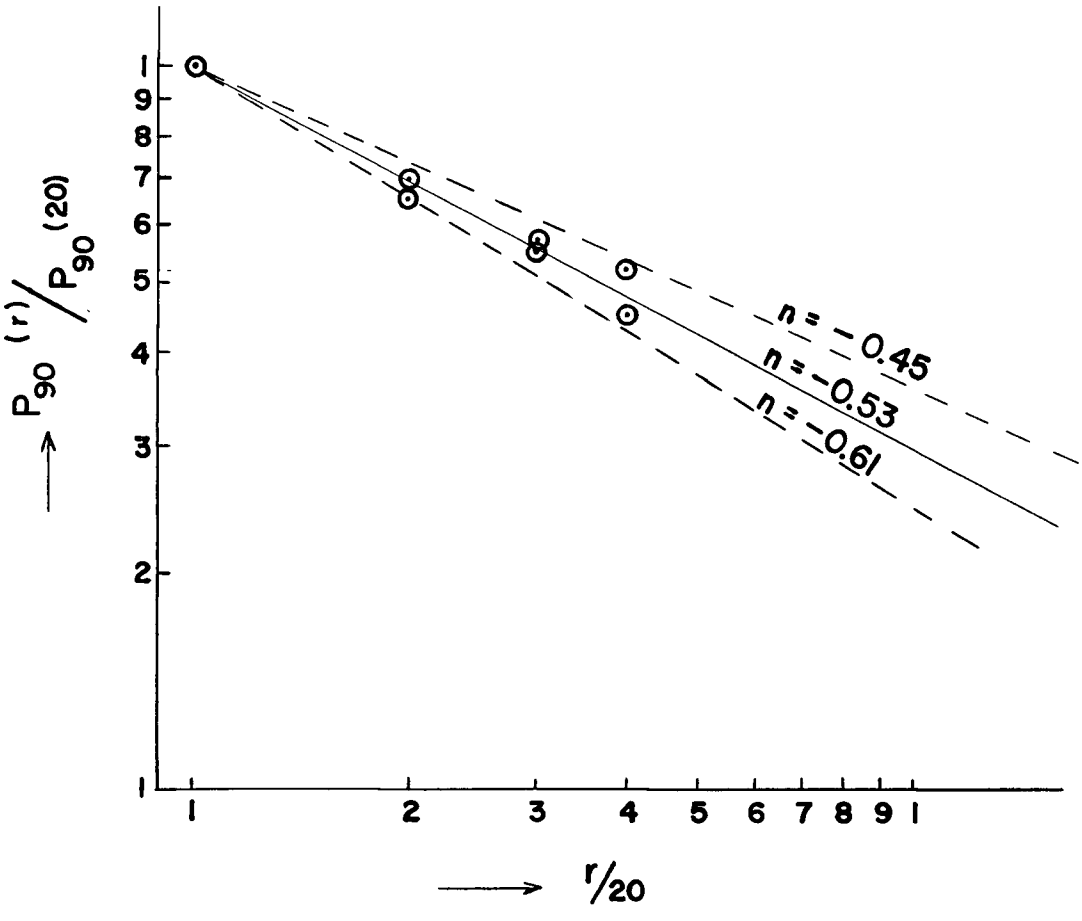

Fig. 17. Attenuation of P waves at 90° from Initial Fractures. The slope is n. The dashed lines are n ± the standard error.

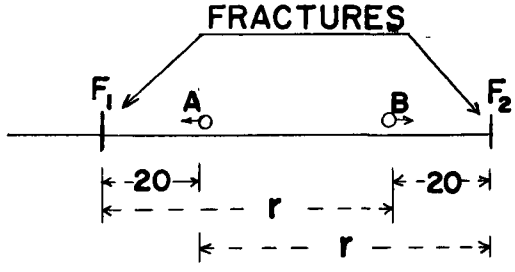

Fig. 16. Transducer and fracture positions for the determination of the far-field region.

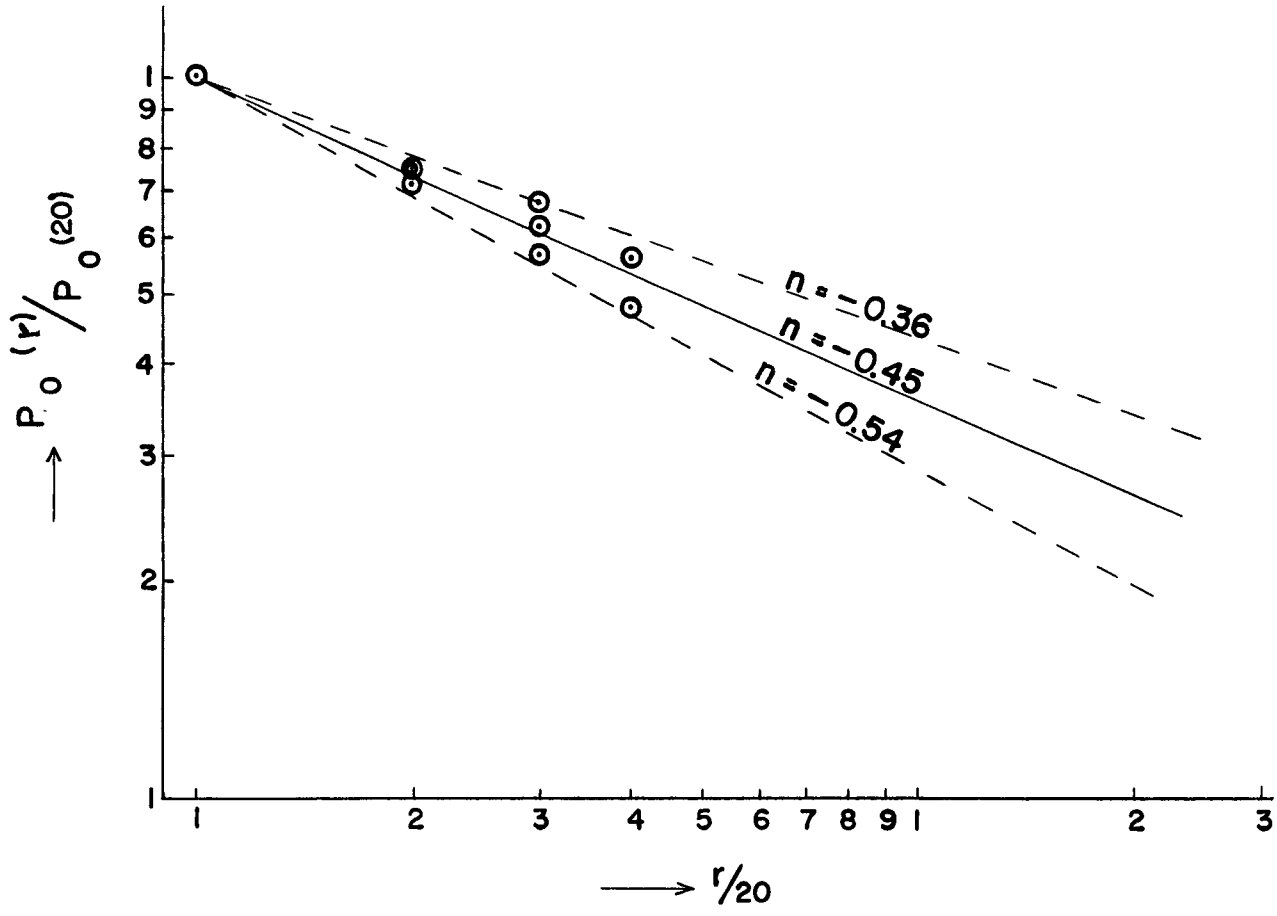

Fig. 18. Attenuation of P waves at 0° from Initial Fractures.

DESCRIPTION OF FIGURES 19, 20, 21 and 22.

Traces of actual records.

Each figure shows four traces on which amplitude measurements are necessary for a single P_θ / P_{90} or S_θ / P_θ ratio measurement. The letter A or B in the parentheses shows the particular transducer used to record the particular trace. The top two traces are records from a fracture F_1. The lower two traces are from a fracture F_2 with the transducer functions interchanged (see figures 14 and 15).

In figures 19, 20 and 21 the typical three extrema waveform of P is seen. In the second trace of figure 20, a kink signified the arrival of the S wave, which is followed by a three extrema waveform. The kink is absent in the third trace, and only two of the three extrema are seen as the trace went off scale.

Referring to figures 14 and 15, we see that the first P motion is always outwards, in figures 19, 20 and 21. The first S motion is always away from the fracture, towards the normal to it.

Figure 22 shows the difficulty of identifying S waves from Extended fracture in the rear quadrant. The frequency is low, the exact arrivals are indistinct, and

amplitude measurements are difficult to make.

There is a higher noise level in figures 21 and 22 because the signals from Extended fractures are amplified 2.5 times more than signals from Initial fractures.

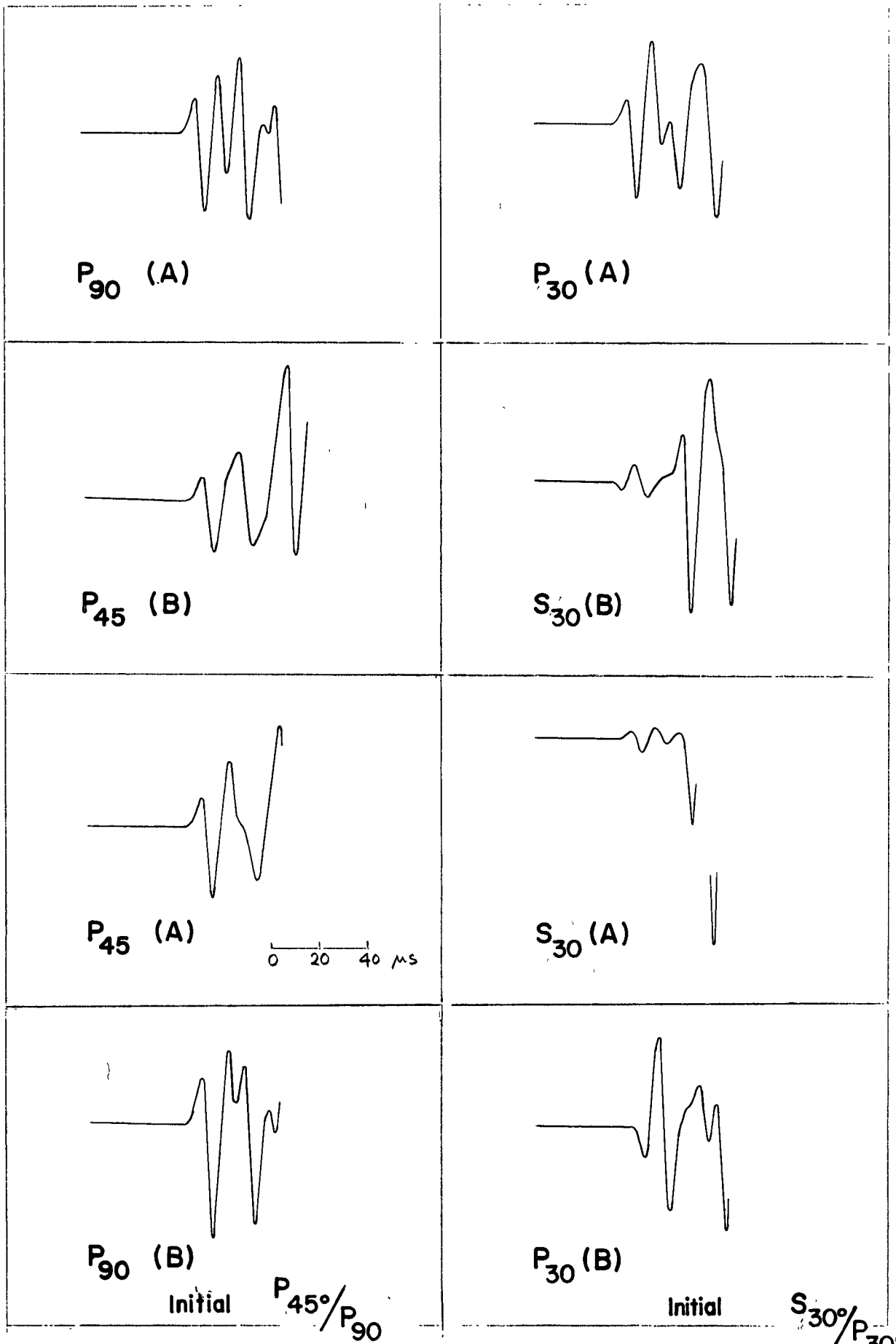

Fig. 19.

Fig. 20.

(See description on page 83)

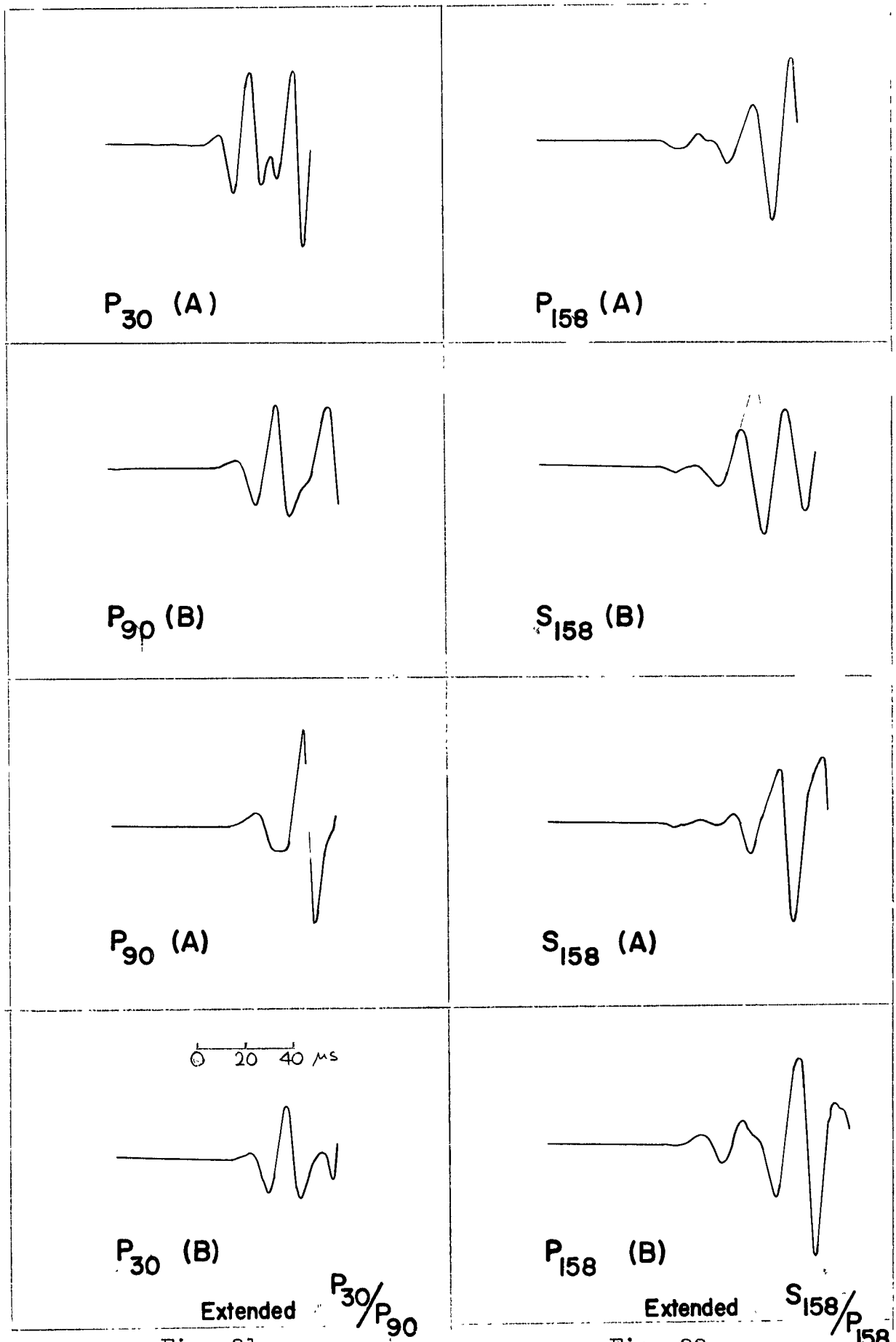

Fig. 21. Fig. 22.

(See description on pages 83-84)

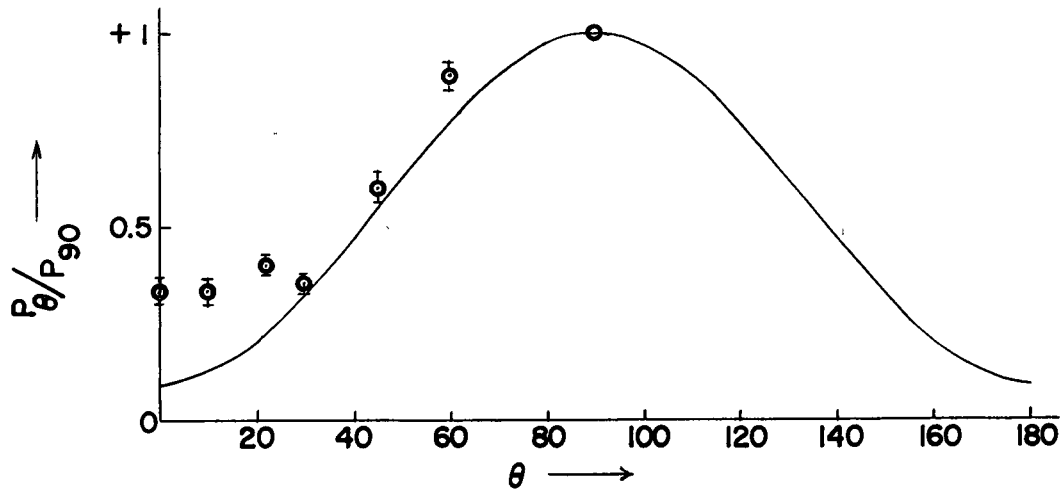

Fig. 23. Plot of measured P_θ/P_{90} ratios from Initial Fractures. Each point is the mean of several measurements. The vertical line represents standard deviation of the mean. The theoretical curve is shown for comparison.

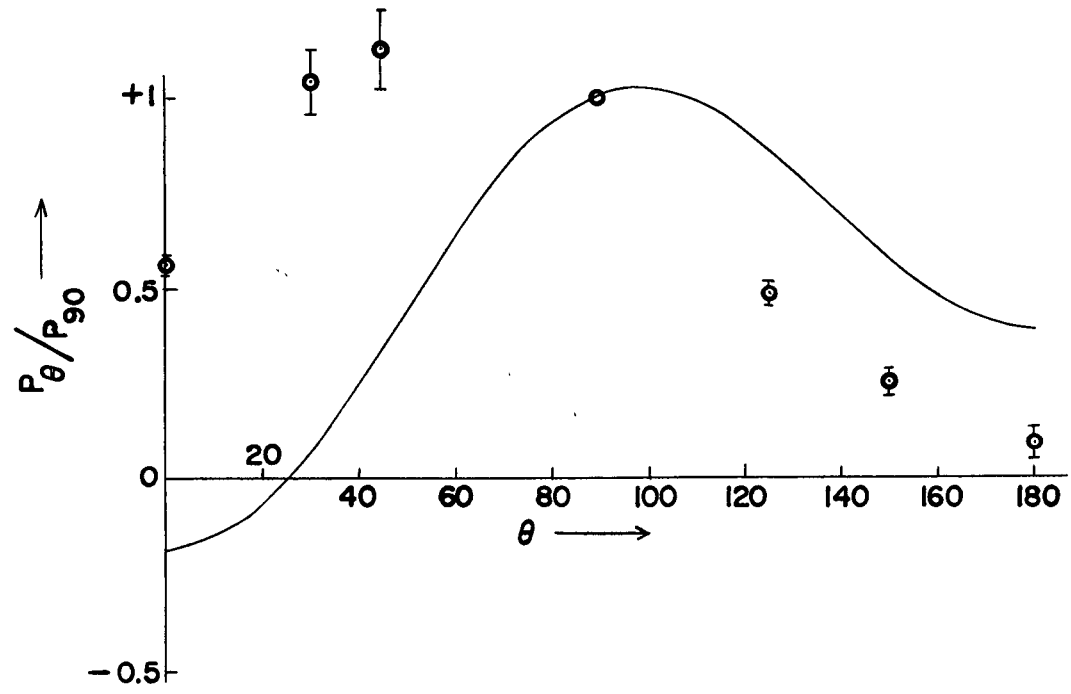

Fig. 25. Plot of measured P_θ/P_{90} ratios from Extended Fractures.

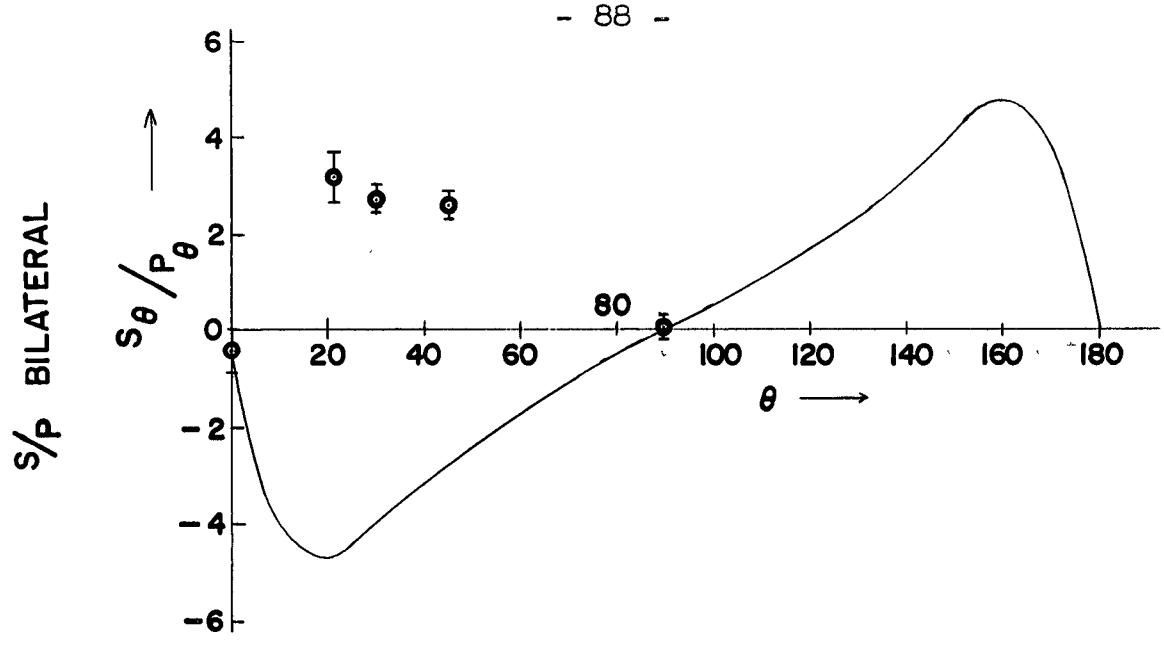

Fig. 24. Plot of measured S_θ / P_θ ratios from Initial Fractures.

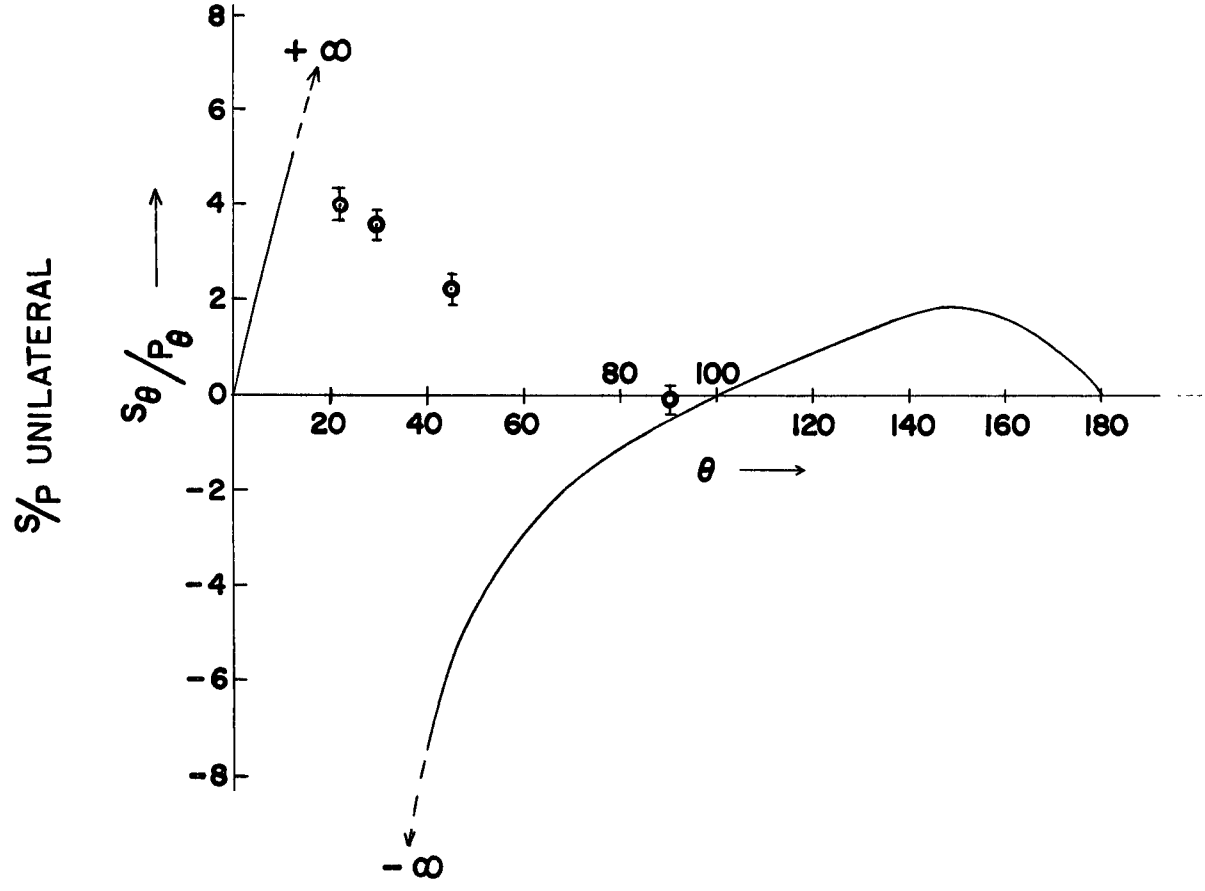

Fig. 26. Plot of measured S_θ / P_θ ratios from Extended fractures.

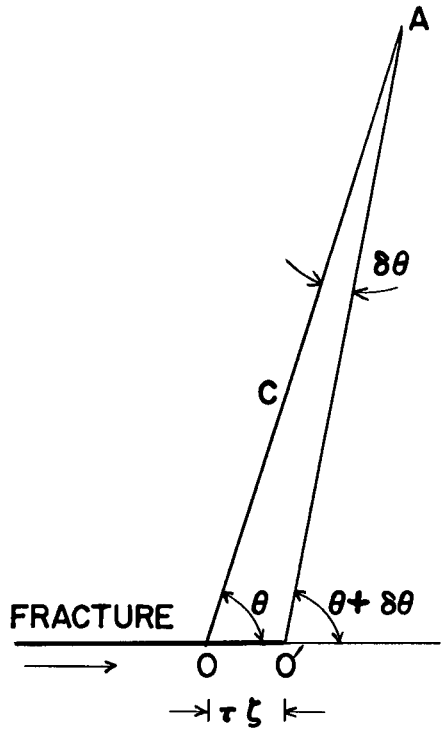

Fig. 27. Figure showing change of θ with propagation of the fracture.

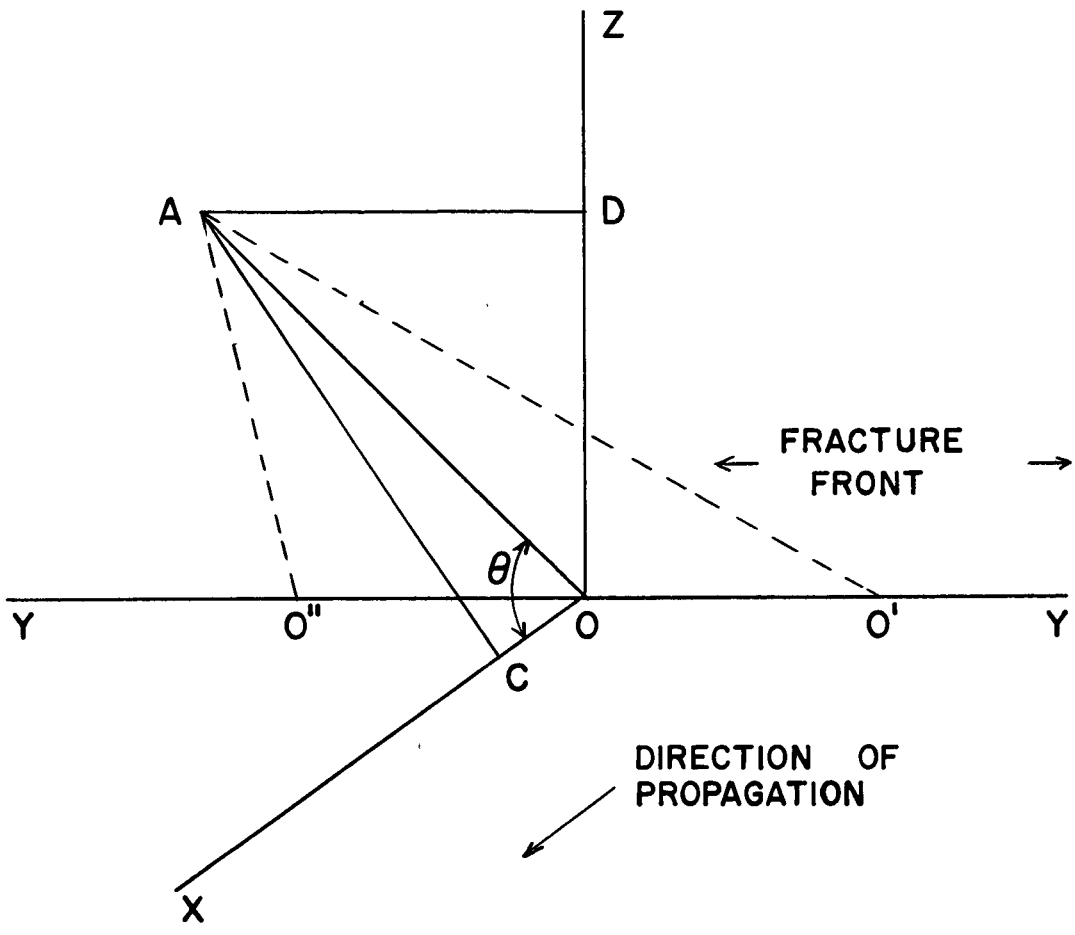

Fig. 28. Figure shows contributing segment of infinite fracture front.

TABLE I
(see Figure 14)

θ	ψ	d	f
0°	45°	21.1	21.1
10°	40°	23	19.3
22.5°	33.8	25	16.7
30°	30	26	15
45°	22.5	27.75	11.5
60°	15	28.9	7.8
90°	0	30	0

TABLE II

P_θ / P_{90} Ratio for Initial Fractures

θ	n	P_θ/P_{90}	Mean	Standard Deviation	Standard Deviation of the Mean	Theory
0	5	0.30 0.31 0.32 0.26 0.45	0.33	0.07	0.03	0.09
10	5	0.26 0.34 0.42 0.29 0.36	0.33	0.06	0.03	0.13
22.5	5	0.43 0.47 0.36 0.42 0.34	0.40	0.05	0.02	0.23
30	5	0.37 0.30 0.34 0.41 0.32	0.35	0.04	0.02	0.31
45	5	0.55 0.66 0.65 0.50 0.62	0.60	0.07	0.03	0.55
60	5	0.98 0.92 0.83 0.90 0.80	0.89	0.07	0.03	0.77
90		1.00	Normalizing Point			1.00

TABLE III

S_θ / P_θ Ratios for Initial Fractures

θ	n	S_θ/P_θ	Mean	Standard Deviation	Standard Deviation of the Mean	Theory
22.5	8	2.40 2.82 1.83 1.82 2.28 3.85 5.48 4.13	3.05	1.30	0.46	- 4.59
30	9	2.67 2.62 2.00 2.18 3.27 4.02 2.19 3.74 1.85	2.73	0.78	0.26	- 4.16
45	5	2.79 1.94 2.05 3.30 2.75	2.57	0.57	0.25	- 2.72
90	4	- 0.56 0.12 0.15 0.00	- 0.07	0.33	0.16	0.00

TABLE IV

P_θ / P_{90} Ratio for Extended Fractures

θ	n	P_θ / P_{90}	Mean	Standard Deviation	Standard Deviation of the Mean	Theory
0	3	0.55 0.52 0.60	0.56	0.04	0.02	- 0.19
30	4	0.84 0.97 1.21 1.12	1.04	0.16	0.08	0.07
45	3	1.03 1.31 1.02	1.12	0.16	0.09	0.35
90		1.00	Normalizing Point			1.00
135	3	0.45 0.54 0.46	0.48	0.05	0.03	0.75
150	4	0.23 0.16 0.29 0.32	0.25	0.07	0.04	0.56
180	3	0.15 0.00 0.08	0.08	0.07	0.04	0.38

TABLE V

S_θ / P_θ Ratios for Extended Fractures

θ	n	S_θ / P_θ	Mean	Standard Deviation	Standard Deviation of the Mean	Theory
22.5	7	5.00 3.14 4.83 2.70 4.10 4.63 3.03	3.92	0.95	0.36	43.52
30	5	3.36 3.50 3.09 4.03 3.34	3.46	0.35	0.16	-24.33
45	4	2.60 1.80 1.80 2.60	2.20	0.46	0.23	- 5.55
90	4	- 0.36 0.10 0.31 - 0.50	- 0.11	0.38	0.19	- 0.62
135) 150) 158)		No acceptable records.				

TABLE VI

Calculated S_θ / P_{90} Ratios for Initial Fractures

θ	S_θ / P_{90}	Standard Deviation σ	Standard Deviation of the Mean σ_μ	Theory
22.5	1.22	1.35	0.48	- 1.05
30	0.96	0.82	0.28	- 1.29
45	1.54	0.64	0.28	- 1.46
90	- 0.07	0.33	0.16	0.00

TABLE VII

Calculated S_θ / P_{90} Ratios for Extended Fractures

θ	S_θ / P_{90}	Standard Deviation σ	Standard Deviation of the Mean σ_μ	Theory
30	3.60	0.51	0.24	- 1.61
45	2.46	0.62	0.32	- 1.93
90	- 0.11	0.38	0.19	- 0.62

The following relations have been used:

$$S_\theta / P_{90} = \left[S_\theta / P_\theta\right] \times \left[P_\theta / P_{90}\right]$$

$$\sigma = \sigma\left(S_\theta / P_\theta\right) + \sigma\left(P_\theta / P_{90}\right)$$

$$\sigma_\mu = \sigma_\mu\left(S_\theta / P_\theta\right) + \sigma_\mu\left(P_\theta / P_{90}\right)$$

APPENDIX I

STRESS FIELD OF AN AXIALLY SYMMETRICAL TEMPERATURE GRADIENT IN A THIN PLATE

It is of some interest to calculate the stress distribution in a thin plate which is heated over a small circular area. Clearly the temperature field will be axially symmetric. We use T to denote the temperature above the ambient room temperature and η to denote the linear coefficient of thermal expansion. The stress-strain relation is given by the Duhamel-Neumann law, which, subject to the assumption of plane stress ($\sigma_z = 0$) may be written as

$$\epsilon_r = \frac{1}{E}(\sigma_r - \nu\sigma_\theta) + \eta T \qquad \text{I-1}$$

$$\epsilon_\theta = \frac{1}{E}(\sigma_\theta - \nu\sigma_r) + \eta T \qquad \text{I-2}$$

Two of the equilibrium equations are satisfied identically by virtue of the foregoing assumptions; the other equation is

$$-\frac{d\sigma_r}{dr} + \frac{\sigma_r - \sigma_\theta}{r} = 0 \qquad \text{I-3}$$

This equation is satisfied by the stress function Φ if

$$\sigma_r = \frac{\Phi}{r} \quad \text{and} \quad \sigma_\theta = \frac{d\Phi}{dr} \qquad \text{I-4}$$

The compatibility equation for rotational symmetry is

$$r\frac{d\epsilon_\theta}{dr} + \epsilon_\theta - \epsilon_r = 0 \qquad \text{I-5}$$

Substituting I-1, I-2, and I-4 into equation I-5 we get

$$\frac{d^2\Phi}{dr^2} + \frac{1}{r}\frac{d\Phi}{dr} - \frac{\Phi}{r^2} = -\eta E \frac{dT}{dr}$$

or

$$\frac{d}{dr}\left\{\frac{1}{r}\frac{d}{dr}(r\Phi)\right\} = -\eta E \frac{dT}{dr} \qquad \text{I-6}$$

Integrating the above, we obtain

$$\Phi = \frac{-\eta E}{r}\int_0^r Tr\, dr + \frac{K_1 r}{2} + \frac{K_2}{r} \qquad \text{I-7}$$

Replacing Φ in I-4 with expression I-7 we have

$$\sigma_r = \frac{-\eta E}{r^2}\int_0^r Tr\, dr + \frac{K_1}{2} + \frac{K_2}{r^2} \qquad \text{I-8}$$

$$\sigma_\theta = \eta E\left\{-T + \frac{1}{r^2}\int_0^r Tr\, dr\right\} + \frac{K_1}{2} - \frac{K_2}{r^2} \qquad \text{I-9}$$

For finite stresses at the center K_2 must be zero. The normal stress must vanish as $r \longrightarrow \infty$. Thus for any normal temperature distribution (i.e. $T \longrightarrow 0$, as $r \longrightarrow \infty$)

$$K_1 = 0 \qquad \text{I-10}$$

The final expressions for σ_r and σ_θ are

$$\sigma_r = -\frac{\eta E}{r^2} \int_0^r Tr \, dr \qquad \text{I-11}$$

$$\sigma_\theta = \eta E \left\{ -T + \frac{1}{r^2} \int_0^r Tr \, dr \right\} \qquad \text{I-12}$$

To evaluate the integrals, we need determine T as a function of r. For this we use the computations of Jaeger (1955) and Carlslaw and Jaeger (1959). Jaeger has given the solutions for the case in which an inner region of radius 'a' is held at a constant temperature for time $t > 0$ and gives tables for the variation of T against r for various time t. Experimental measurements made upon a glass plate heated by a gas flame for approximately 45 seconds indicated 'a' to be about 0.5 cms and T about 200° C.

Initial fractures start between 30 seconds and 60 seconds after the application of a gas flame to the plate. We have used the mean value of 45 seconds for our calculations. The physical properties of the glass used are

Thermal conductivity	-	0.0028 cal/sec cm ^{o}C
Coefficient of Linear expansion	-	85 x 10^{-7}
Specific heat	-	0.20 cal/gm ^{o}C
Density	-	2.5 gm/ cm^{3}
Diffusivity	-	5.6 x 10^{-3} cm^{2} /sec

We assume a uniform temperature from r = o to r = 0.5 cm. The variation of T(r) versus r for t = 45 secs is given in figure 7; the variation of σ_r and σ_θ with r at t = 45 secs is given in figure 8, in the main text.

APPENDIX II

PLATE WAVES

Oliver, Press and Ewing (1954) first noted that it would be possible to use elastic waves in thin plates to study problems of seismic wave propagation. The principal result of their study was that the symmetric plate wave in a thin plate was the analog of the dilatational wave in a solid. There is, however, a stringent requirement that the plate thickness be sufficiently small compared with the wavelength studied.

Extensive investigations of the vibrations of a thin plate have been published by Rayleigh (1889), Lamb (1917), Tolstoy and Usdin (1953), Oliver, Press and Ewing (1954), and Ewing, Jardetzky and Press (1957). We reproduce here those results which are important in the problem studied here.

The following notation has been used:

u,v,w	displacement in the X, Y, Z directions respectively.
σ_{xy} etc.	stress acting in the X direction on a plane normal to the Y axis.
θ	dilatation

Φ and Ψ - displacement potentials

ρ - density

λ, μ - Lame's constants

α^2 - $\frac{\lambda + 2\mu}{\rho}$

β^2 - $\frac{\mu}{\rho}$

Let us consider a thin plate bounded by the planes $z = \pm h$, with the X and Y axes in the median plane of the plate. The thickness of the plate is, then, 2h. The plate can be considered infinite in extent, with the bounding surfaces free of normal and tangential stresses. Following Rayleigh (1889) we assume that all periodic functions in the solutions of the equations of motion involve x only through e^{-ikx} and y does not appear at all. This implies that while the displacement in the y direction is finite, $\frac{\partial \Theta}{\partial y} = 0$.

We will have two sets of solutions:

I. u and w are finite and v vanishes.

II. v is finite and u and w vanish.

Case I. Two dimensional symmetric and antisymmetric vibrations of a thin plate. The displacements can be written in the form

$$u = \frac{\partial \Phi}{\partial x} - \frac{\partial \Psi}{\partial z} \quad , \quad w = \frac{\partial \Phi}{\partial z} + \frac{\partial \Psi}{\partial x} \qquad \text{II-1}$$

where the potentials Φ and Ψ are solutions of the wave equations

$$\nabla^2\Phi = \frac{1}{\alpha^2}\frac{\partial^2\Phi}{\partial t^2} \quad , \quad \nabla^2\Psi = \frac{1}{\beta^2}\frac{\partial^2\Psi}{\partial t^2} \qquad \text{II-2}$$

The boundary conditions are that the stresses must vanish across the free surface. Thus

$$\left.\begin{aligned} \sigma_{zz} &= \lambda\Theta + 2\mu\frac{\partial w}{\partial z} = 0 \\ \sigma_{zx} &= \mu\left(\frac{\partial w}{\partial x} + \frac{\partial u}{\partial z}\right) = 0 \\ \sigma_{zy} &= \mu\left(\frac{\partial w}{\partial y} + \frac{\partial v}{\partial z}\right) = 0 \end{aligned}\right\} \text{ at } z = \pm h \qquad \text{II-3}$$

We assume a solution of the form

$$\Phi = (A\sinh \nu z + B\cosh \nu z)\, e^{i(\omega t - kx)}$$

$$\Psi = (C\sinh \nu' z + D\cosh \nu' z)\, e^{i(\omega t - kx)} \qquad \text{II-4}$$

where $\nu^2 = k^2 - k_\alpha^2$, $\nu'^2 = k^2 - k_\beta^2$, $k_\alpha = \frac{\omega}{\alpha}$, $k_\beta = \frac{\omega}{\beta}$

On substituting equation II-4 in II-1 and II-3, we obtain the equations

$$\frac{\tanh \nu h}{\tanh \nu' h} = \frac{4 k^2 \nu \nu'}{(\nu'^2 + k^2)^2} \qquad \text{II-5}$$

$$\frac{\tanh \nu h}{\tanh \nu' h} = \frac{(\nu'^2 + k^2)^2}{4 k^2 \nu \nu'} \qquad \text{II-6}$$

The coefficients A and D can be separated from B and C. Now we can consider a motion <u>symmetric</u> with respect to plane z = 0 which is given by

$$\left.\begin{aligned} \Phi &= B \cosh \nu z \; e^{i(\omega t - kx)} \\ \Psi &= C \sinh \nu' z \; e^{i(\omega t - kx)} \end{aligned}\right\} \qquad \text{II-7}$$

For waves long compared with the thickness 2h, the products kh, νh, ν'h may be considered small. The equation II-6 reduces to

$$(\nu'^2 + k^2)^2 - 4 k^2 \nu^2 = 0 \qquad \text{II-8}$$

From this we obtain the velocity of plate longitudinal waves as

$$\frac{c^2}{\beta^2} = 4\left(1 - \frac{\beta^2}{\alpha^2}\right) = \frac{4(\lambda+\mu)}{(\lambda+2\mu)} = \frac{C^2_{plate}}{\beta^2}$$

Therefore $$C_p^2 = 4\frac{\mu}{\rho}\frac{(\lambda+\mu)}{(\lambda+2\mu)} \qquad \text{II-9}$$

The anti-symmetric motion is given by the functions

$$\varphi = A \sinh \nu z \; e^{i(\omega t - kx)}$$

$$\psi = D \cosh \nu' z \; e^{i(\omega t - kx)} \qquad \text{II-10}$$

Antisymmetric motion (otherwise known as flexural waves) involves bending of the plate. For waves long compared with 2h the equation II-6 reduces to

$$\frac{c^2}{\beta^2} = \frac{4}{3}(kh)^2\left(1 - \frac{\beta^2}{\alpha^2}\right) \qquad \text{II-11}$$

These waves are dispersive, the phase velocity decreasing to zero for long wavelengths.

Case II. Another solution involves only motion in the plane of the plate. Thus w = 0. The same boundary conditions II-3 apply. Consider the equation of motion

$$\rho \frac{\partial^2 v}{\partial t^2} = (\lambda + \mu) \frac{\partial \Theta}{\partial y} + \mu \nabla^2 v \qquad \text{II-12}$$

As $\frac{\partial \Theta}{\partial y}$ is zero, we find that the displacement v itself satisfies the wave equation. The equation is

$$\frac{\partial^2 v}{\partial t^2} = \frac{\mu}{\rho} \nabla^2 v$$

The velocity is given by $\sqrt{\frac{\mu}{\rho}}$ which is the shear wave velocity in infinite solids. The solution is of the form

$$v = (P \sinh \nu' z + Q \cosh \nu' z)\, e^{i(\omega t - kx)} \qquad \text{II-13}$$

To satisfy the boundary conditions of $\frac{\partial v}{\partial z} = 0$ either P = 0, in which case

$$v = Q \cosh \nu' z \qquad \text{II-14}$$

or Q = 0, whence

$$v = P \sinh \nu' z \qquad \text{II-15}$$

Oliver, Press and Ewing (1954) have established the equivalence between the long wave approximation of

the first plate mode and dilatational waves in a thin plate. Thus, it has been shown that shear and dilatational waves exist in thin plates. The velocity of shear waves in thin plates is the same as for infinite medium, while the velocity of the plate dilatational wave is modified. For long wavelengths, the velocity of flexural waves is small, and this type of plate wave motion arrives so late that it does not interfere with plate dilatational and shear waves in two dimensional modelling.

BIBLIOGRAPHY

Benioff, H., F. Press and S. Smith (1961). Excitation of the free oscillations of the earth by earthquakes. J. Geop. Res. vol. 66, p.605.

Ben-Menahem, A. (1961). Radiation of seismic surface waves from finite moving sources. Bull. Seis. Soc. Am., vol. 51, p.401.

Carlslaw, H.S. and J.C. Jaeger. "Conduction of Heat in Solids", Oxford Univ. Press, Oxford, 1959, p.334.

de Hoop, A.T. (1958). Representation theorems for the displacement in an elastic solid and their application to elastodynamic diffraction theory. D. Sc. Thesis, Delft.

Evans, J.F., C.F. Hadley, J.D. Eisler and D. Silverman (1954). A three-dimensional seismic wave model with both electrical and visual observation of waves. Geop., vol. 19, p.220.

Ewing, M., W. Jardetzky and F. Press "Elastic waves in layered media". New York, McGraw-Hill, 1957. p.281.

Griffith, A.A. (1920). The phenomenon of rupture and flow in solids. Phil. Trans. Roy. Soc. London. A. vol. 221, p.163.

Healy, J.H. and F. Press (1959). Further model study of the radiation of elastic waves from a dipole source. Bull. Seis. Soc. Am., vol. 49, p. 193.

Howes, E.T., L. H. Tejada-Flores and L. Randolph (1953). Seismic model study. J. Acous. Soc. Am., vol.25, p. 915.

Inglis, C.E. (1913). Stresses in a place due to the presence of cracks and sharp corners. Trans. Inst. Naval Arch., vol. 60, p.219.

Irwin, G.R. "Fracture". Handbuch der Physik, vol.6, p.551. Berlin, Springer-Verlag 1958.

Jaeger, J.C. (1955). Numerical values for the temperature in radial heat flow. J. Math. and Phys., vol. 34, p.316.

Joffe, E.H. (1951). The moving Griffith crack. Phil. Mag., vol. 42, part 2, p.739.

Kasahara, K. Experimental Studies on the mechanism of generation of elastic waves.
I (1952) Bull. Eqke. Res. Inst. Tokyo U., vol. 30, p. 259
II (1953) vol. 31, p. 71
III (1953) vol. 31, p. 235
IV (1954) vol. 32, p. 67
V (1955) vol. 33, p. 411

Kato, Y. and A. Takagi (1956). Seismic model studies: On the initial motion of dilatational and distortional waves produced by various types of forces. Sci. Rep. Tohoku U., vol. 8, p.212.

Knopoff, L. (1955). Small three-dimensional seismic models. Trans. Am. Geop. U, vol. 36, p.1029.

Knopoff, L. (1956). Diffraction of elastic waves. J.Acous. Soc. Am., vol 28, p.217.

Knopoff, L. and F. Gilbert (1959). Radiation from a strike slip fault. Bull. Seis. Soc. Am., vol.49, p. 163.

Knopoff, L. and F. Gilbert (1960). First motions from seismic sources. Bull Seis. Soc. Am., vol.50, p.117.

Lamb, H. (1917). On waves in an elastic plate. Proc. Roy. Soc. London., A. vol. 93, p.114.

Levin, F.K. and H.C. Hibbard (1955). Three dimensional seismic model studies. Geop., vol. 20, p. 19.

O'Brien, P.N.S. (1955). Model seismology - critical refraction of elastic waves. Geop. vol.20, p.227.

Oliver, J., F. Press and M. Ewing (1954). Two dimensional model seismology. Geop., vol.19, p. 202.

Press, F. (1957). Elastic wave radiation from a fault. J. Acous. Soc. Am., vol. 29, p. 187.

Press, F. (1957). Elastic wave radiation from faults in ultrasonic models. Publ. Dom. Obs. Ottawa, vol.20 p. 271.

Press, F., A. Ben-Menahem and M. N. Koksoz (1961). Experimental determination of earthquake fault length and rupture velocity. J. Geop. R., vol.66, p. 3471.

Press, F., J. Oliver and M. Ewing (1954). Seismic model study of refraction from a layer of finite thickness. Geop., vol. 19, p. 388.

Rayleigh, Lord (1889). On the free vibrations of an infinite plate of homogeneous isotropic elastic matter. Proc. Lond. Math. Soc., vol.20, p. 225.

Schardin, H. "Velocity Effects in Fracture". "Fracture", Averbach et al, editors. p. 297. New York, John Wiley & Sons, 1959.

Schardin, H. and W. Struth (1937). Neuere Ergebnisse der Funkenkinematographie. Z. Tech. Phys., vol. 18, p. 474.

Tatel, H.E. (1954). Note on the nature of a seismogram J. Geop. Res. vol. 59, p. 289.

Tolstoy, I. and E. Usdin (1953). Dispersive properties of stratified elastic and liquid media: A ray theory. Geop., vol. 18, p. 844.

Wang, C.T. "Applied Elasticity". New York, McGraw-Hill, 1953.

Wells, A.A. and D Post (1958). The dynamic stress distribution surrounding a running crack. Proc. Soc. Exper. Stress. Analysis, vol. 16, p.69.

Westergaard, H.M. (1939). Bearing pressures and cracks. J. App. Mech., Trans. ASME. vol. 61, pp. A-49-53.

Williams, M.L. (1956). On the stress distribution at the base of a stationary crack. J. App. Mech., Trans. ASME. vol. 79, p. 109.